Search for an $I = 3$ dibaryon resonance

Takatsugu Ishikawa[a] and Hiroaki Ohnishi

Research Center for Electron Photon Science (ELPH),

Tohoku University, Sendai, Miyagi 982-0826, Japan

Jung Keun Ahn

Department of Physics, Korea University, Seongbuk, Seoul 02841, Korea

Takaya Akaishi

Department of Physics, Osaka University, Toyonaka, Osaka 560-0043, Japan

Wen-Chen Chang

Institute of Physics, Academia Sinica, Taipei 11529, Taiwan

Hiroyuki Fujioka

Department of Physics, Tokyo Institute of Technology, Meguro, Tokyo 152-8551, Japan

Ryotaro Honda and Masashi Kaneta

Department of Physics, Tohoku University, Sendai, Miyagi 980-8578, Japan

Youichi Igarashi and Kyoichiro Ozawa

Institute of Particle and Nuclear Studies (IPNS),

High Energy Accelerator Research Organization (KEK), Tsukuba, Ibaraki 305-0801, Japan

Yue Ma and Takumi Yamaga

Nishina Center for Accelerator-Based Science,

Institute of Physical and Chemical Research (RIKEN), Wako, Saitama 351-0198, Japan

Megumi Naruki

Department of Physics, Kyoto University, Kyoto, Kyoto 606-8502, Japan

Hiroyuki Noumi, Kotaro Shirotori, Yorihito Sugaya, Natsuki Tomida, and Masaru Yosoi

Research Center for Nuclear Physics (RCNP),

Osaka University, Ibaraki, Osaka 567-0047, Japan

Chary Rangacharyulu

Department of Physics and Engineering Physics,

University of Saskatchewan, Saskatoon, Saskatchewan S7N 5E2, Canada

Takahiro Sawada

Department of Physics, Osaka City University, Osaka, Osaka 558-8585, Japan

Kiyoshi Tanida

Advanced Science Research Center (ASRC),

Japan Atomic Energy Agency (JAEA), Tokai, Ibaraki 319-1195, Japan

Abstract

We propose an experiment to search for an $I = 3$ dibaryon resonance $\mathcal{D}_{30}$ using the $pp \to \pi^-\pi^-\mathcal{D}_{30}^{++++} \to \pi^-\pi^-(\pi^+\pi^+pp)$ reaction at the several incident proton momenta around 3–4 GeV/c (Dibaryon states are denoted by $\mathcal{D}_{IJ}$, where I and J stand for the isospin and spin). The $d^*(2380)$ resonance observed at the WASA-at-COSY collaboration can be attributed to the spatially-compact six-quark hadron state and/or isoscalar ($I = 0$) $\Delta\Delta$ quasi-bound state $\mathcal{D}_{03}$, which is predicted as a member of sextet dibaryons by Dyson and Xuong six decades ago. If the $d^*(2380)$ resonance with $I(J^\pi) = 0(3^+)$ is $\mathcal{D}_{03}$, a resonance corresponding to $\mathcal{D}_{30}$ with $I(J^\pi) = 3(0^+)$ must be observable in the $I = 3$ $\Delta\Delta$ invariant-mass distribution. The $p(p, \pi^-\pi^-)X$ reaction provides X with charge $Q = +4$ and baryon number $B = 2$, giving an $I = 3$ state and leaving $\pi^+\pi^+pp$ in the final state. The WASA-at-COSY collaboration tried to search for $\mathcal{D}_{30}$ by using this reaction, but they cannot separate the produced $\mathcal{D}_{30}^{++++}$ events from the background phase-space contribution because of a lack of statistics coming from the very small acceptance owing to the low particle-identification power. In this proposal, we measure the cross sections for the $pp \to \pi^-\pi^-\pi^+\pi^+pp$ reaction to search for $\mathcal{D}_{30}$ at several incident proton momenta around 3–4 GeV/c with huge statistics and large acceptance for detecting all the final-state particles using the general-purpose E50 detector system. When the existence of $\mathcal{D}_{30}$ is confirmed, all the sextet (ground-state) dibaryons are established. The measured mass and width also provide information on the $\Delta\Delta$ interaction.

PACS numbers: 13.60.Le, 14.80. - j

[a] Spokesperson: ishikawa@lns.tohoku.ac.jp

EXECUTIVE SUMMARY

reaction:	$pp \to \pi^-\pi^-\pi^+\pi^+pp$
beamline:	high-intensity high-momentum secondary beamline
beam:	protons with an average intensity of 1 MHz
	(2-s spill, 5.2-s cycle; unseparated positively-charged particles)
target:	liquid hydrogen with a thickness of 570 mm
detector:	the E50 spectrometer
beamtime:	3 days for 2.85 GeV/c
	3 days for 3.35 GeV/c
	3 days for 3.60 GeV/c
	3 days for 3.80 GeV/c
	3 days for 4.00 GeV/c

We measure the cross sections for the $pp \to \pi^-\pi^-\pi^+\pi^+pp$ reaction to search for $\mathcal{D}_{30}^{++++}$ dibaryon resonance at several incident proton momenta around 3–4 GeV/c with huge statistics and large acceptance for detecting all the final-state particles. It is important to measure cross sections at several incident momenta for studying the background contributions, and confirming a possible $\mathcal{D}_{30}^{++++}$ contribution when we observe some resonance-like behavior in the $p(p, \pi^-\pi^-)$ missing mass or $\pi^+\pi^+pp$ invariant-mass distributions. We assume the thickness of the liquid hydrogen target is 570 mm. If it is shorter than we plan, an additional beam time is required. The high-intensity high-momentum secondary beamline is expected to be constructed step by step. Since the required beam intensity of protons is only 1 MHz, corresponding to the 0.5-kW loss (1/30 of the final goal) of the primary beam at the production target, the proposed experiment can be performed before the E50 experiment becomes ready.

I. INTRODUCTION

The internal structure of a color-neutral object, hadron, is a subject in the non-perturbative domain of quantum chromodynamics (QCD). The familiar mesons and baryons are composed of $q\bar{q}$ and qqq, respectively. More complex quark configurations beyond them are objects of great interest to investigate the effective degrees of freedom describing hadrons and to understand color confinement. Among them, a dibaryon has become an interesting object since the quark picture of a nucleon was established [1]. A phase change of the basic configuration of dibaryon states is expected from a molecule-like state consisting of two baryons (such as the deuteron) to a hexaquark hadron state, which could appear as a spatially-compact exotic particle. Understanding dibaryons would not only give a clue to the solution of the current problem in hadron physics, but also provide an insight into the nuclear equation of state and the interior of a neutron star [2].

Dyson and Xuong predicted the sextet of non-strange dibaryons $\mathcal{D}_{IJ}$ with isospin I and spin J: $\mathcal{D}_{01}$, $\mathcal{D}_{10}$, $\mathcal{D}_{12}$, $\mathcal{D}_{21}$, $\mathcal{D}_{03}$, and $\mathcal{D}_{30}$ [3]. Table I summarizes the sextet dibaryons predicted by Dyson and Xuong. They provided these masses in a simple form:

$$\begin{aligned} M =& A + \{I(I+1) - J(J+1) - 2\}\, B \\ & \text{with } A = 1878 \text{ MeV and } B = 47 \text{ MeV} \end{aligned} \tag{1}$$

using the those of the three experimentally observed states: the deuteron $\mathcal{D}_{01}$, the ${}^1S_0$-NN virtual state $\mathcal{D}_{10}$, and a resonance-like structure corresponding to $\mathcal{D}_{12}$ which appears at $M = 2.16$ GeV in the $\pi^+ d \to pp$ reaction [4].

TABLE I. Sextet dibaryons predicted by Dyson and Xuong. The composition of each dibaryon state is described in terms of the nucleon N and delta baryon Δ. The mass of dibaryon M is expressed by $M = A + \{I(I+1) - J(J+1) - 2\}\, B$ with two parameters: $A = 1878$ MeV and $B = 47$ MeV.

dibaryon	$\mathcal{D}_{01}$	$\mathcal{D}_{10}$	$\mathcal{D}_{12}$	$\mathcal{D}_{21}$	$\mathcal{D}_{03}$	$\mathcal{D}_{30}$
component	NN	NN	ΔN	ΔN	$\Delta\Delta$	$\Delta\Delta$
mass form	A	A	$A+6B$	$A+6B$	$A+10B$	$A+10B$
mass value	1.88 GeV	1.88 GeV	2.16 GeV	2.16 GeV	2.35 GeV	2.35 GeV

The first non-NN-composed dibaryon $\mathcal{D}_{12}$ is a candidate of a ΔN quasi-bound state, which is given as the ${}^3P_2$ multipole strength at $M = 2.18$ GeV in $\pi^{\pm}d$ elastic scattering by a partial-wave analysis [5]. The corresponding ${}^1D_2$-pp amplitude also shows the same structure in the $\pi^+d \to pp$ reaction [6]. Fig. 1 shows the Argand plot of the dominant πd partial waves for $\pi^{\pm}d$ elastic scattering, and that of the dominant pp partial waves for the $\pi^+d \to pp$ reaction. The ${}^3P_2$-πd and ${}^1D_2$-pp partial waves are clearly observed as the strongest amplitude. The SAID group provides the pole of $\mathcal{D}_{12}$ [7] from a combined analysis of $\pi^{\pm}d$ elastic scattering, the $\pi^+d \to pp$ reaction, and pp elastic scattering. Apparently, the peak is observed at a center of mass (CM) energy corresponding to the sum of the Δ and N masses. However, the dibaryonic interpretations of the experimental data for $\mathcal{D}_{12}$ have been questionable since quasi-free Δ production cannot be kinematically separated. The recent observation of a sequential decay of an isoscalar dibaryon into $\pi\mathcal{D}_{12}$ confirms the dibaryonic interpretation of $\mathcal{D}_{12}$ [8], which will be discussed later.

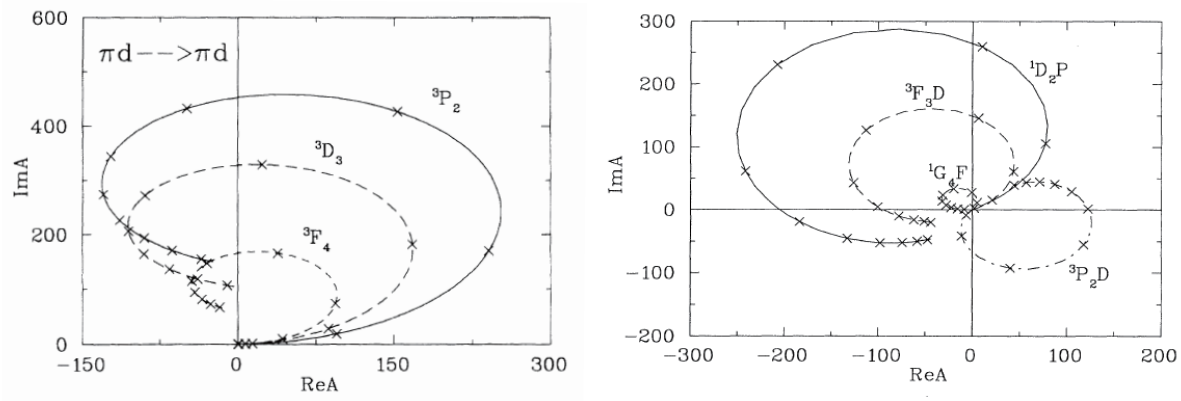

FIG. 1. Argand plot of the dominant πd partial waves for $\pi^{\pm}d$ elastic scattering (left), and that of the dominant pp partial waves for the $\pi^+d \to pp$ reaction (right). The πd partial waves of ${}^3P_2$, ${}^3D_3$, and ${}^3F_4$ correspond to ${}^1D_2$-, ${}^3F_3$-, and ${}^1G_4$-pp states, respectively. The data points are plotted with a 50-MeV step, and all the amplitudes are multiplied by 10^3. The ${}^3P_2$-πd state and ${}^1D_2$-pp state would be attributed to $\mathcal{D}_{12}$. The data are taken from Ref. [5] in the left panel, and from Ref. [6] in the right panel.

The next observed non-NN-composed dibaryon is an isoscalar $\Delta\Delta$ quasi-bound state $\mathcal{D}_{03}$. Kamae *et al.* obtained the first indication in 1977 [9, 10]. They found the resonance-like behavior in the polarization of emitted protons at the CM energy of 2.35 GeV in the deuteron photo-disintegration, and discussed the possibility of the existence of $\mathcal{D}_{03}$. The

A2 collaboration at Mainz MAMI has studied this behavior in the Σ beam asymmetry for the same reaction in detail recently, and confirmed the multipole strength corresponding to $\mathcal{D}_{03}$ [11].

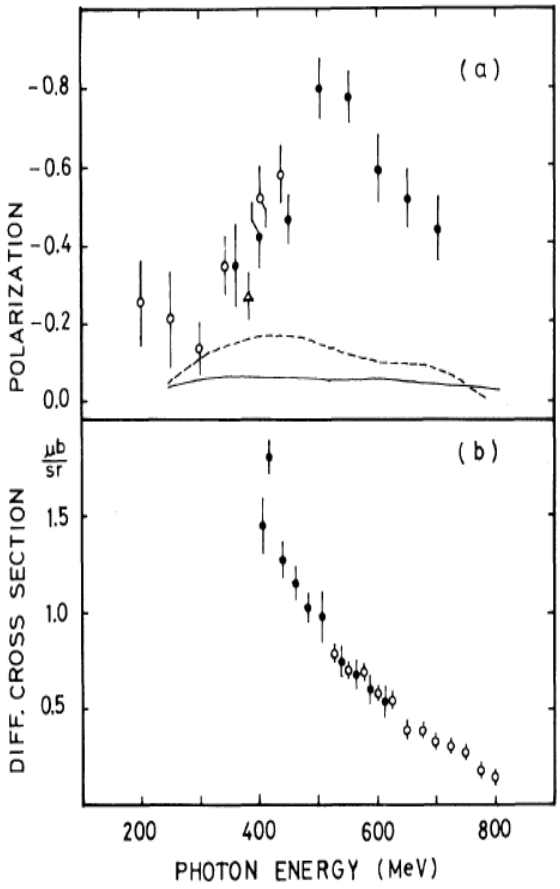

FIG. 2. Proton polarization (upper) and differential cross section (lower) at 90° in the CM frame as a function of the incident photon energy. A resonance-like structure is observed in the proton polarization although neither bump nor peak is formed in the differential cross section at the corresponding photon energy. The data are taken from Ref. [9].

The CELSIUS/WASA collaboration obtained a clear evidence of the isoscalar resonance called $d^*(2380)$ in the $pn \to \pi^0\pi^0 d$ reaction [12]. Successively, the WASA-at-COSY collaboration confirmed its existence in the same reaction, and gave the mass $M \simeq 2.37$ GeV and width $\Gamma \simeq 0.07$ GeV [13]. Fig. 3 shows the total cross section as a function of the pn-CM energy and πd invariant-mass distribution for the $pn \to \pi^0\pi^0 d$ reaction measured by the WASA-at-COSY collaboration. The $d^*(2380)$ resonance may be attributed to $\mathcal{D}_{03}$. Its existence seems to solve a long standing puzzle called the ABC effect that a higher-^{3}He-

momentum enhancement (corresponding to the lower two-pion invariant-mass close to the sum of two pion masses) is observed for the $pd \to (\pi\pi)_{I=0}\,{}^3\mathrm{He}$ reaction [14, 15] and similar observations. Additionally, the possibility is discussed that $d^*(2380)$ production explains a dilepton spectroscopy puzzle [16]. The e^+e^- invariant mass observed in the heavy-ion collision shows an enhancement below the ρ^0 and ω masses [17]. One of the interpretations to this enhancement is the medium modification of vector mesons, but the decay of $d^*(2380) \to \Delta\Delta \to \rho^0 NN$ can also explain the enhancement since the ρ^0 mass is lower than its central value in this decay.

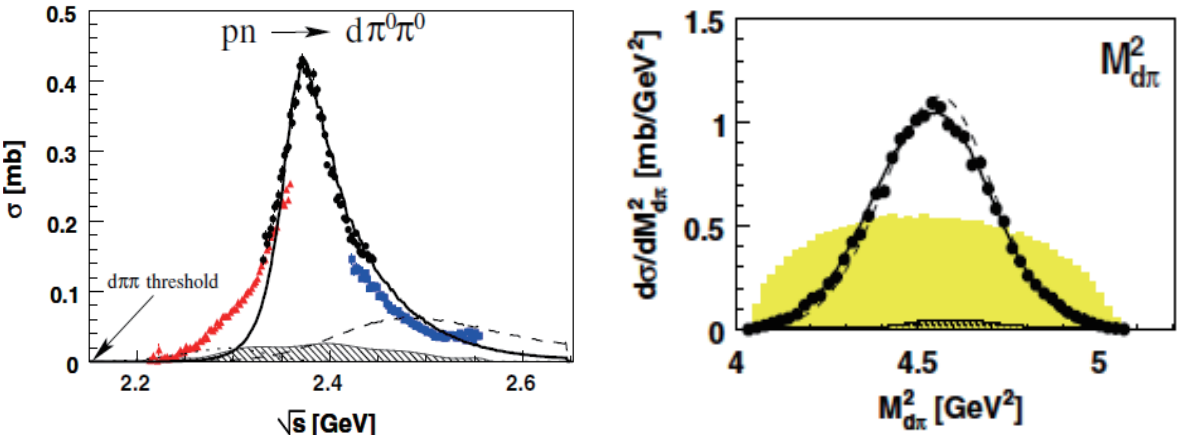

FIG. 3. Total cross section as a function of the CM energy for the $pn \to \pi^0\pi^0 d$ reaction measured by the WASA-at-COSY collaboration (left). The triangle (red), circles (black), and squares (blue) correspond to the data obtained at incident proton energies of 1.0, 1.2, and 1.4 GeV, respectively. The hatched area indicates systematic uncertainties. The solid curve represents the contribution from an s-channel resonance with a mass of 2.37 GeV and width of 68 MeV. $\pi^0 d$ invariant-mass distribution (differential cross section as a function of square of the $\pi^0 d$ invariant mass) at the CM energy of 2.38 GeV (right). The hatched and shaded areas represent systematic uncertainty and phase-space distribution, respectively. The $d^*(2380)$ resonance seems predominantly decay into an isovector resonance with a mass of 2.15 GeV by emitting π^0. The data are taken from Ref. [13].

The WASA-at-COSY collaboration confirmed the existence of $d^*(2380)$ not only in the $pn \to \pi^0\pi^0 d$ reaction [13] but also in the $pn \to \pi^+\pi^- d$ reaction [18], and gave the mass $M \simeq 2.37$ GeV and width $\Gamma \simeq 0.07$ GeV. In addition to the $\pi^0\pi^0 d$ and $\pi^+\pi^- d$ final states, $d^*(2380)$ has been observed in the $\pi^0\pi^- pp$ [19], $\pi^0\pi^0 pn$ [20], and $\pi^+\pi^- pn$ [21] final states.

The SAID partial-wave analysis, which incorporates the analyzing power for quasi-elastic $\vec{n}+p \to n+p$ scattering, provides the quantum numbers $I(J^\pi) = 0(3^+)$ [22, 23] for $d^*(2380)$. All the observations except for the first evidence have beem made by the WASA-at-COSY collaborations. Fig. 4 shows the $d^*(2380)$ resonance observed by the WASA-at-COSY collaboration in the various final states. These experimental results have stimulated intensive

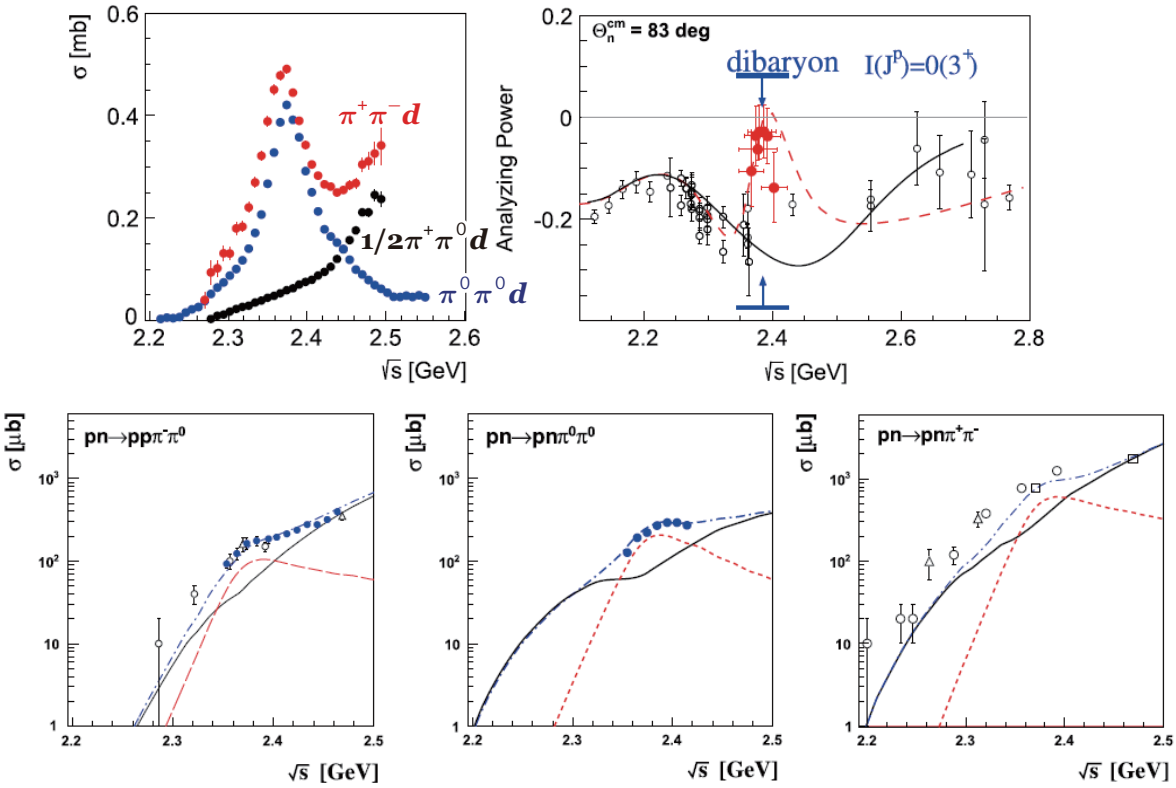

FIG. 4. $d^*(2380)$ signals observed by the WASA-at-COSY collaboration in the various final states. The total cross sections are presented as a function of the CM energy for the $pn \to \pi^+\pi^- d$ reaction [18] (upper left), $pn \to \pi^0\pi^- pp$ [19] (lower left), $pn \to \pi^0\pi^0 pn$ [20] (lower middle), and $pn \to \pi^+\pi^- pn$ [21] (lower right) reactions. The analyzing power is plotted for the quasi-elastic $\vec{n} + p \to n + p$ scattering at 83° in the CM frame [22, 23] (upper right). The total cross section for $pn \to \pi^+\pi^- d$ is well-reproduced by a sum of that for the isoscalar $pn \to \pi^0\pi^0 d$ channel and a half of that for the isovector $pp \to \pi^+\pi^0 d$ channel in the upper-left panel. Each $NN\pi\pi$ channel show a shoulder corresponding to $d^*(2380)$ represented by the dashed curve (red) in the lower three panels. The analyzing power shows a sudden change at 2.38 GeV in the upper-right panel, suggesting its quantum numbers are $I(J^\pi) = 0(3^+)$.

theoretical investigations of $\mathcal{D}_{03}$ [24, 25]. The $d^*(2380)$ is claimed as a mixed state between 33% of a two-baryon molecule-like state and 66% of a hexaquark state [26, 27]. Although the structure of $d^*(2380)$ is not established yet, the decay $\mathcal{D}_{03} \to \pi\mathcal{D}_{12}$ seems dominant [28].

The s-channel photoproduction of $d^*(2380)$ has also been investigated as a first step to know the size of $d^*(2380)$. Both the $\gamma d \to \pi^+\pi^- d$ reaction at JLAB/CLAS [29] and $\gamma d \to \pi^0\pi^0 d$ reaction at ELPH/FOREST [8, 30] do not give a clear evidence for $d^*(2380)$ production. However, the experimentally obtained cross sections suggest the sequential $\gamma d \to \mathcal{D}_{0\mathrm{J}} \to \pi\mathcal{D}_{12} \to \pi\pi d$ reaction with an isoscalar dibaryon $\mathcal{D}_{0J}$ and an isovector dibaryon $\mathcal{D}_{12}$. Fig. 5 shows the total cross section as a function of the γd-CM energy (the excitation function) for the $\gamma d \to \pi^0\pi^0 d$ reaction at incident energies from 0.57 to 1.15 GeV. In addition to a slight enhancement corresponding to $d^*(2380)$, two new isoscalar-dibaryon states are claimed at 2.47 and 2.63 GeV. Neither quasi-free $\pi^0\pi^0$ nor π^0 photoproduction with

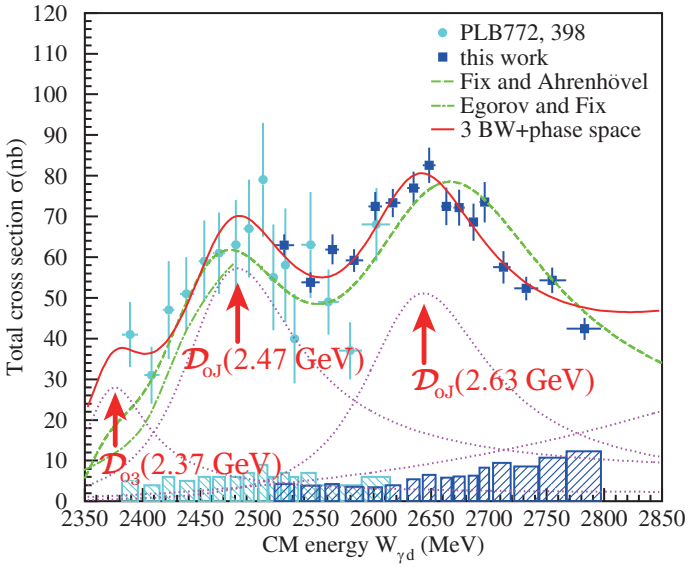

FIG. 5. Total cross section as a function of the γd-CM energy for the $\gamma d \to \pi^0\pi^0 d$ reaction at incident energies from 0.57 to 1.15 GeV. The dashed and dotted-dashed curves represent the calculations by Fix and Ahrenhövel [31] and by Egorov and Fix [32], respectively, based on quasi-free $\pi^0\pi^0$ photoproduction with a deuteron coalescence. Although these theoretical calculations well reproduces the total cross sections, they cannot reproduce the angular distribution of deuteron emission at all. The sequential $\gamma d \to \mathcal{D}_{0J} \to \pi^0\mathcal{D}_{12} \to \pi^0\pi^0 d$ reaction are suggested from the data with an isoscalar dibaryon $\mathcal{D}_{0J}$ and an isovector dibaryon $\mathcal{D}_{12}$. The data are taken from Ref. [8].

a deuteron coalescence can reproduce the angular distribution of deuteron emission at all. Therefore, the intermediate state must be an isovector dibaryon $\mathcal{D}_{12}$, which is the same as the ${}^3P_2$-πd and ${}^1D_2$-pp partial waves observed in $\pi^{\pm}d$ elastic scattering and the $\pi^+ d \to pp$ reaction. The new two states observed in the excitation function at 2.47 and 2.63 GeV might be excited states of the sextet dibaryon members.

In addition to the observation of a $\mathcal{D}_{03}$ candidate $d^*(2380)$, an enhancement corresponding to an isotensor ΔN dibaryon $\mathcal{D}_{21}$ is observed in the quasi-free $pp \to \pi^-\pi^+pp$ reaction [33]. Fig. 6 shows the π^+p, π^+pp, π^-p, and π^-pp invariant-mass distributions for the $pp \to \pi^-\pi^+pp$

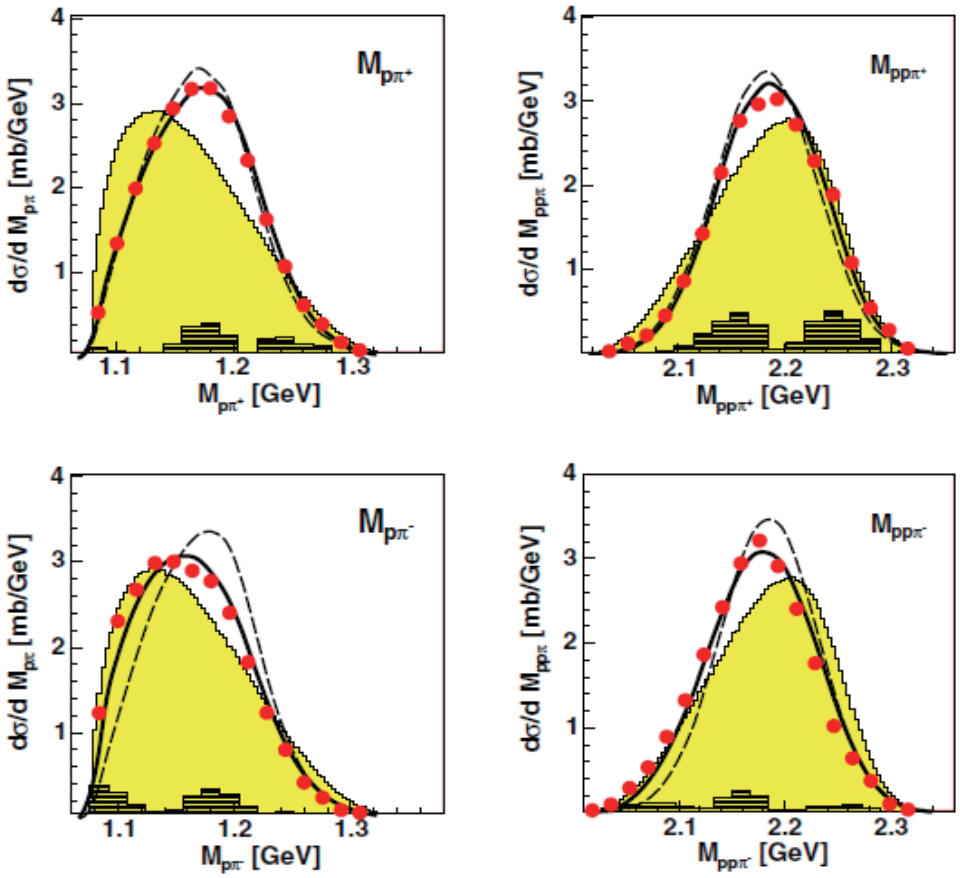

FIG. 6. π^+p (upper left), π^+pp (upper right), π^-p (lower left), and π^-pp (lower right) invariant-mass distributions for the $pp \to \pi^+\pi^-pp$ reaction at incident energies from 0.9 to 1.3 GeV. The shaded area represent pure phase-space distributions, the dashed curves show the theoretical calculation without any $\mathcal{D}_{21}^{++}$ contribution, and the solid curves represent the calculation including the $pp \to \pi^-\mathcal{D}_{21}^{++} \to \pi^+\pi^-pp$ process. The data are taken from Ref. [33].

reaction at incident energies from 0.9 to 1.3 GeV. The deviations from the pure phase-space distributions suggest the existence of $\mathcal{D}_{21}$.

To understand the internal structure of dibaryons, it is important to establish the excitation spectrum and provide their sizes. In this proposal, we focus on the former item, and we will prepare another proposal of an experiment for the latter one. Many experimental investigations of the sextet members for non-strange dibaryons have been made. Although candidates for almost all the members seem to be found, those for the $\mathcal{D}_{30}$ member are still missing. If the $d^*(2380)$ resonance with $I(J^\pi) = 0(3^+)$ is $\mathcal{D}_{03}$, a resonance corresponding to $\mathcal{D}_{30}$ with a $I(J^\pi) = 3(0^+)$ (a mirrored-quantum-number state) must be observable in the $(\Delta\Delta)_{I=3}$ invariant-mass distribution. Table II summarizes the theoretically predicted masses for the $\mathcal{D}_{03}$ and $\mathcal{D}_{30}$ dibaryons. In addition, the $\mathcal{D}_{30}$ is closely related to the $\Omega^-\Omega^-$ system in the $^1S_0$ channel [39], which is predicted as the most strange dibaryon by the HAL QCD collaboration [40]. This $\Omega^-\Omega^-$ dibaryon systems is a loosely-bound state with a binding energy of 1.6 MeV, of which all the u (d) quarks are replaced with s quarks in $\mathcal{D}_{30}^{++++}$ ($\mathcal{D}_{30}^{----}$). In this regard, the $^1S_0$-$\Omega^-\Omega^-$ dibaryon is considered to belong to the same multiplet as $\mathcal{D}_{30}$.

TABLE II. Predicted masses for the $\mathcal{D}_{03}$ and $\mathcal{D}_{30}$ dibaryons. DX, MAS, OY, MT, and GG denote the values obtained by Dyson and Xuong [3], by Mulders, Aerts, and de Swart [35], by Oka and Yazaki [36], by Mulders and Thomas [37], and by Gal and Garcilazo [38], respectively.

dibaryon	DX	MAS	OY	MT	GG	experiment
$\mathcal{D}_{03}$	2.35 GeV	2.361 GeV	2.45 GeV	2.38 GeV	2.38 GeV	2.37 GeV
$\mathcal{D}_{30}$	2.35 GeV	2.833 GeV	unbound	2.69 GeV	2.40 GeV	—

The $\mathcal{D}_{30}$ dibaryon is isospin-decoupled from the NN system. To reach such a state by NN collisions, additional particle generation is required. A candidate reaction to search for $\mathcal{D}_{30}$ is $pp \to \pi^-\pi^-\mathcal{D}_{30}^{++++} \to \pi^-\pi^-\,(\Delta^{++}\Delta^{++}) \to \pi^-\pi^-\,(\pi^+p)\,(\pi^+p)$. The WASA-at-COSY collaboration has investigated this reaction to search for $\mathcal{D}_{30}^{++++}$, and reported no clear evidence [34]. This is because a large amount of the background contribution together with a lack of statistics, coming from the very small acceptance owing to the low particle-identification power, disturbs them to extract the $\mathcal{D}_{30}$-produced events.

We first consider the same reaction to confirm the existence of $\mathcal{D}_{30}$ as the WASA-at-COSY collaboration adopted. They use the incident proton energy of 2.063 and 2.541 GeV, corresponding to the momentum of 2.85, and 3.35 GeV/c, respectively. They cannot separate the produced $\mathcal{D}_{30}^{++++}$ events from the background six-body ($\pi^-\pi^-\pi^+\pi^+pp$) phase-space contribution owing to a lack of statistics. The main purpose of the experiment by the WASA-at-COSY collaboration described in Ref. [34] was ω and η' production, and the data acquired are not suitable for investigating $\mathcal{D}_{30}^{++++}$. At first, the trigger of the data acquisition (DAQ) system required that more than one charged particles were detected in each of the forward and central detectors in WASA. Additionally, a missing-mass trigger was active during the measurements at $T_p = 2.541$ GeV. Since the forward detector was insensitive to the sign of the charge, the events were used that the two protons were detected in the forward detector, and that the four pions were detected in the central detector. Furthermore, particle-identification power is not so high. These conditions made the statistics and acceptance too low. The acceptance of detecting $\pi^-\pi^-\pi^+\pi^+pp$ was only 0.1% and 0.5% at $T_p = 2.063$ and 2.541 GeV, respectively.

The E50 spectrometer we plan to use has much higher tracking efficiency, particle-identification efficiency, and geometrical acceptance for detecting all the final-state particles in the $pp \to \pi^-\pi^-\pi^+\pi^+pp$ reaction. We use several incident momenta around 3–4 GeV/c and acquire the data with huge statistics so that the background contributions can be studied in detail and the possible $\mathcal{D}_{30}$ state can be separated from them. After the existence of $\mathcal{D}_{30}^{++++}$ is confirmed, we can extend the measurement of cross sections using different reactions: $\pi^+d \to \pi^-\pi^-\mathcal{D}_{30}^{++++} \to \pi^-\pi^-\,(\pi^+p\pi^+p)$ and $\pi^-d \to \pi^+\pi^+\mathcal{D}_{30}^{--} \to \pi^+\pi^+\,(\pi^-n\pi^-n)$. By using these π-induced reactions, the two isospin-stretched $\mathcal{D}_{30}$ states can be observed among the seven different charge states ($\mathcal{D}_{30}^{--}, \mathcal{D}_{30}^{-}, \mathcal{D}_{30}^{0}, \ldots, \mathcal{D}_{30}^{++++}$).

II. KINEMATICS

Since we do not know the internal structure of $\mathcal{D}_{30}$, no reliable dominant production mechanism is currently available. However, a loosely-coupled two $N(1440)P_{11}$-nucleon-resonance (the Roper resonance) molecular state may play a role as a doorway to the $\mathcal{D}_{30}$ dibaryon. Fig. 7 shows the possible diagram for $\mathcal{D}_{30}$ production from the pp collision. Two Roper resonances appear in the intermediate state, each of them emits the negative pion, and leaves

the Δ^{++} baryon. The two Δ^{++} baryons are merged into the $\mathcal{D}_{30}^{++++}$ dibaryon finally. It should be noted that each of the two Roper resonances does not necessarily have to satisfy the on-shell condition. The main background contribution would be the independent decay of each Roper resonance into $\pi^-\pi^+p$ and non-resonant six-body ($\pi^-\pi^-\pi^+\pi^+pp$) phase space.

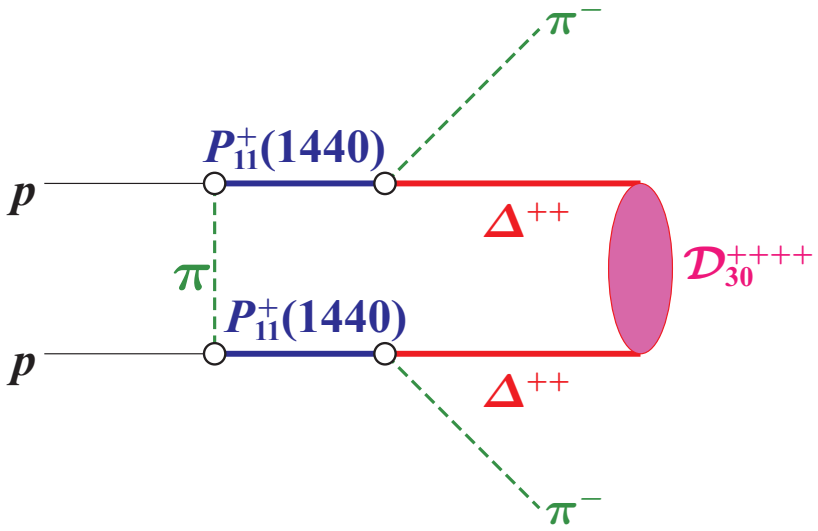

FIG. 7. Possible diagram for $\mathcal{D}_{30}$ production from the pp collision. Two Roper ($N(1440)P_{11}$) resonances would appear in the intermediate state.

The WASA-at-COSY collaboration tried to observe $\mathcal{D}_{30}^{++++}$ using the $pp \to \pi^-\pi^-\pi^+\pi^+pp$ reaction [34] as discussed in the previous section. The $\pi^+\pi^+pp$ invariant-mass distributions show an enhancement corresponding to the possible $\mathcal{D}_{30}^{++++}$-produced events although the collaboration did not conclude the existence of $\mathcal{D}_{30}$. Fig. 8 shows the $\pi^+\pi^+pp$ invariant-mass distributions at the incident energies of 2.063 and 2.541 GeV. A slight enhancement corresponding to $\mathcal{D}_{30}^{++++}$ is observed although it is not statistically significant. We do not know the details of the acceptance of the WASA detector, thus a fraction of the $\mathcal{D}_{30}^{++++}$ yield to all the four-pion produced events is assumed to be common with and without acceptance correction. Of course, the trigger bias must affect the acceptance for detecting all the final-state particles as a function of the $\pi^+\pi^+pp$ invariant mass in the WASA-at-COSY experiment. What we can do is to assume the flatness of the acceptance. The total cross section is found to be roughly 0.037 (0.27) μb for $\mathcal{D}_{30}^{++++}$ production at $T_p = 2.063$ (2.541) GeV, corresponding to the incident proton momentum of 2.85 and 3.35 GeV/c, since

that is 0.7 ± 0.3 (5.2 ± 1.0) μb for the $pp \to \pi^-\pi^-\pi^+\pi^+pp$ reaction.

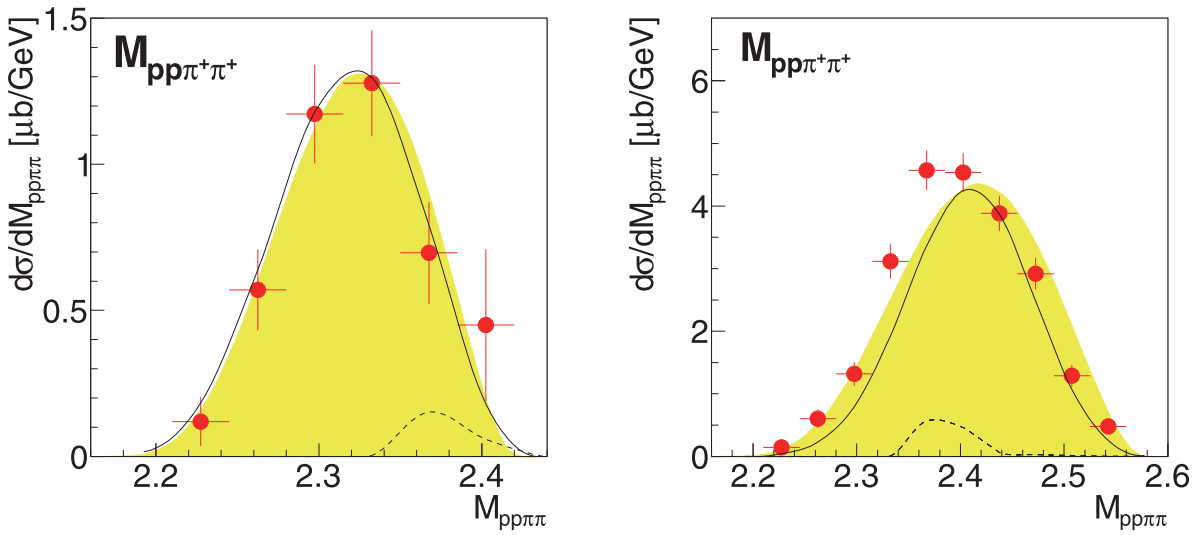

FIG. 8. $\pi^+\pi^+pp$ invariant-mass distributions without acceptance correction at incident energies of 2.063 GeV (left) and 2.541 GeV (right) obtained by the WASA-at-COSY collaboration. The shaded histograms represent the non-resonant phase-space contribution, the solid curve shows the two Roper-resonance production contribution, and the dotted shows the effect of an $I = 3$ resonance with a mass of 2.37 GeV and width of 0.07 GeV. The data are taken from Ref. [34].

We assume the energy dependences of the total cross sections are proportional to the six-body and three-body pure-phase contributions for the $pp \to \pi^-\pi^-\pi^+\pi^+pp$ and $pp \to \pi^-\pi^-\mathcal{D}_{30}^{++++}$ reactions, respectively. Fig. 9 shows the total cross section as a function of the incident proton kinetic energy. The cross sections are normalized to those measured by the WASA-at-COSY collaboration at $T_p = 2.063$ and 2.541 GeV. The incident momenta of 3.6, 3.8, 4.0 and 5.0 GeV/c correspond to the kinetic energy of 2.78, 2.98, 3.17 and 4.15 GeV, respectively. The WASA-at-COSY collaboration can not separate the possible $\mathcal{D}_{30}$ production from the background $pp \to \pi^+\pi^+\pi^-\pi^-pp$ contribution since these contributions are merged into a bump because of a lack of statistics. To separate these components clearly, we can make the $\pi^+\pi^+pp$ invariant-mass distributions with huge statistics and finer bins and/or make the peak position of the background contribution higher by choosing the higher kinetic energy of the proton beam that the WASA-at-COSY collaboration cannot achieve.

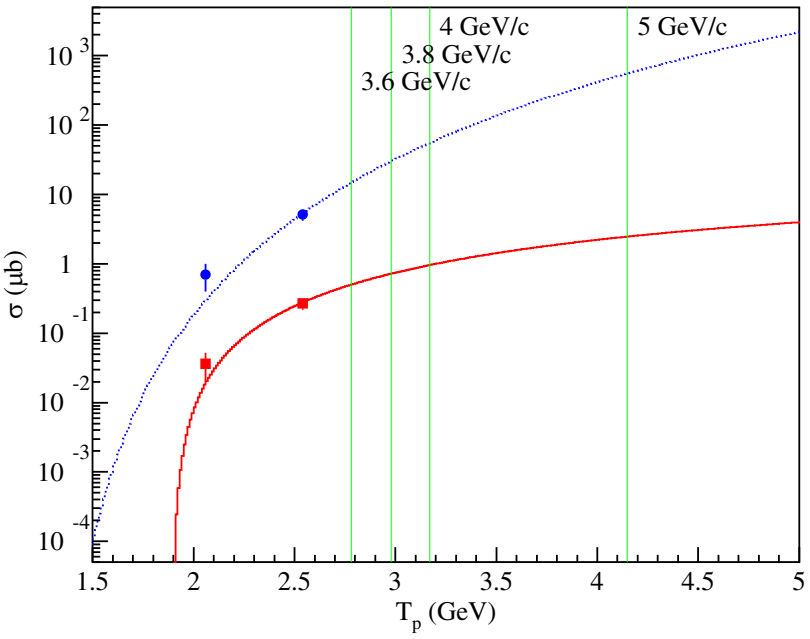

FIG. 9. Total cross section as a function of the incident proton kinetic energy T_p. The dotted curve (blue) shows that for the $pp \to \pi^-\pi^-\pi^+\pi^+pp$ reaction, and the solid curve (red) shows that estimated for the $pp \to \pi^-\pi^-\mathcal{D}_{30}^{++++}$ reaction. The energy dependences of the total cross sections are given by pure six-body and three-body phase-space contributions, respectively, normalized to the data point at $T_p = 2.063$ and 2.541 GeV. The incident energies of $T_p = 2.063$ and 2.541 GeV correspond to the incident proton momenta of 2.85 and 3.35 GeV/c, respectively.

Next, we estimate the missing mass distribution (the differential cross section as a function of the missing mass) for the $pp \to \pi^-\pi^-X$ reaction. The $\pi^+\pi^+\pi^-\pi^-pp$ events are produced according to the pure six-body phase-space, and normalized to the estimated total cross section for the $pp \to \pi^-\pi^-\pi^+\pi^+pp$ reaction. It should be noted that the energy dependence of the incident flux is taken into account. As for $\mathcal{D}_{30}^{++++}$ production, the Breit-Wigner strength with a mass of 2.37 GeV and width of 0.07 GeV is multiplied and normalized to the estimated total cross section for the $pp \to \pi^-\pi^-\mathcal{D}_{30}^{++++}$ reaction. Fig. 10 shows the missing mass distributions for the $pp \to \pi^-\pi^-X$ reaction at the incident proton momentum of 3.6, 3.8, 4.0, and 5.0 GeV/c. The background contribution is very large when the incident momentum is higher than 4.0 GeV/c, and it is difficult to separate the $\mathcal{D}_{30}^{++++}$-produced events and background contribution when the incident momentum is lower than 3.35 GeV.

Thus, the optimum incident momentum is approximately 3.35–3.60 GeV/c.

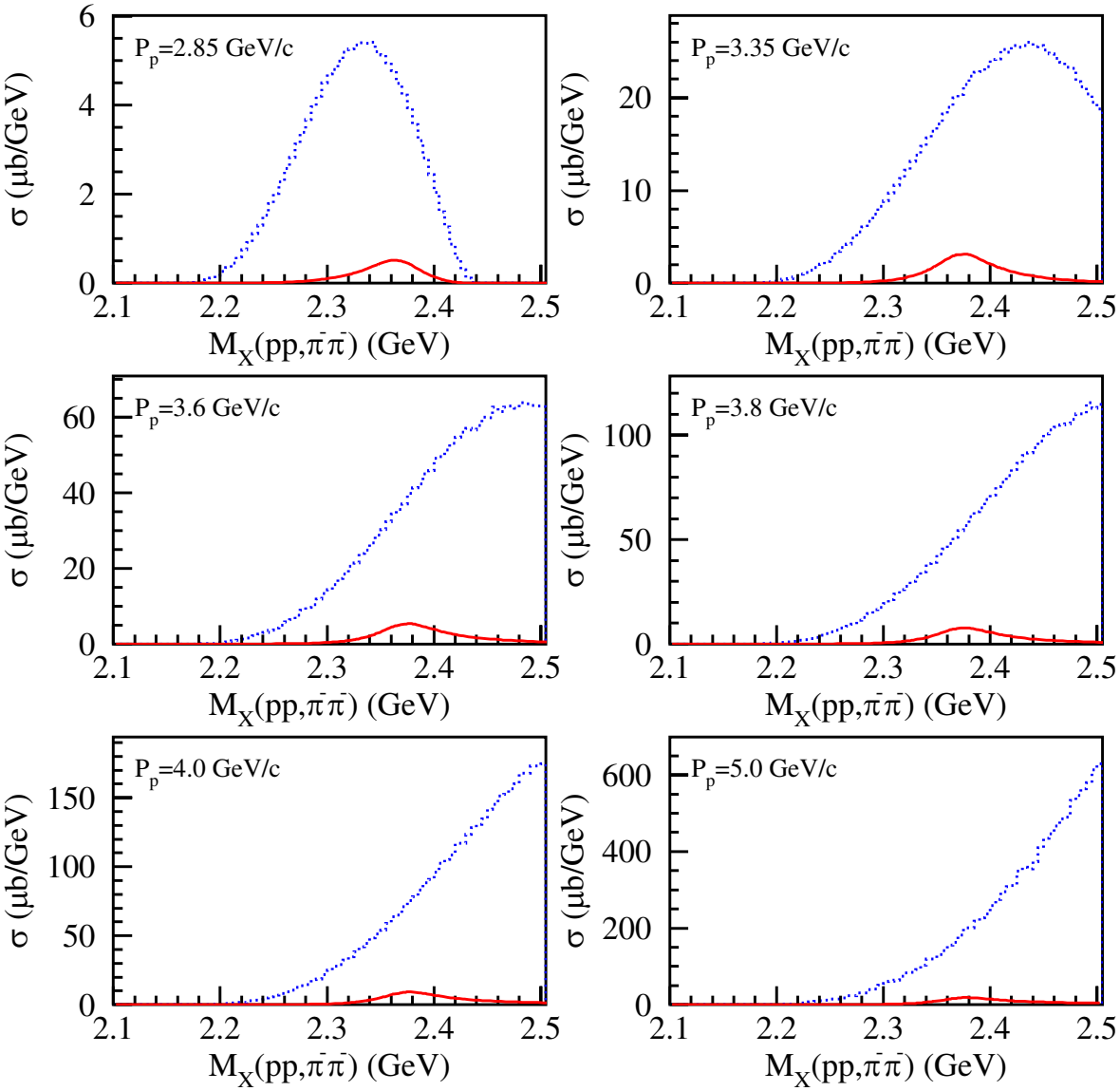

FIG. 10. Missing mass M_X distributions for the $pp \to \pi^-\pi^- X$ reaction at the incident proton momentum of 2.85, 3.35, 3.6, 3.8, 4.0, and 5.0 GeV/c. The dotted curve (blue) shows the background $pp \to \pi^+\pi^+\pi^-\pi^- pp$ contribution, and the solid curve (red) shows the $pp \to \pi^-\pi^-\mathcal{D}_{30}^{++++}$ contribution.

Thus far, the background contribution is assumed to be given by the pure six-body phase-space. Here, we assume the two Roper resonances appear in the intermediate state. We use 1.44 and 0.2 GeV for the mass and width of the resonance, and the total cross section for the background contribution is again normalized to the estimated one. Fig. 11 shows the missing-

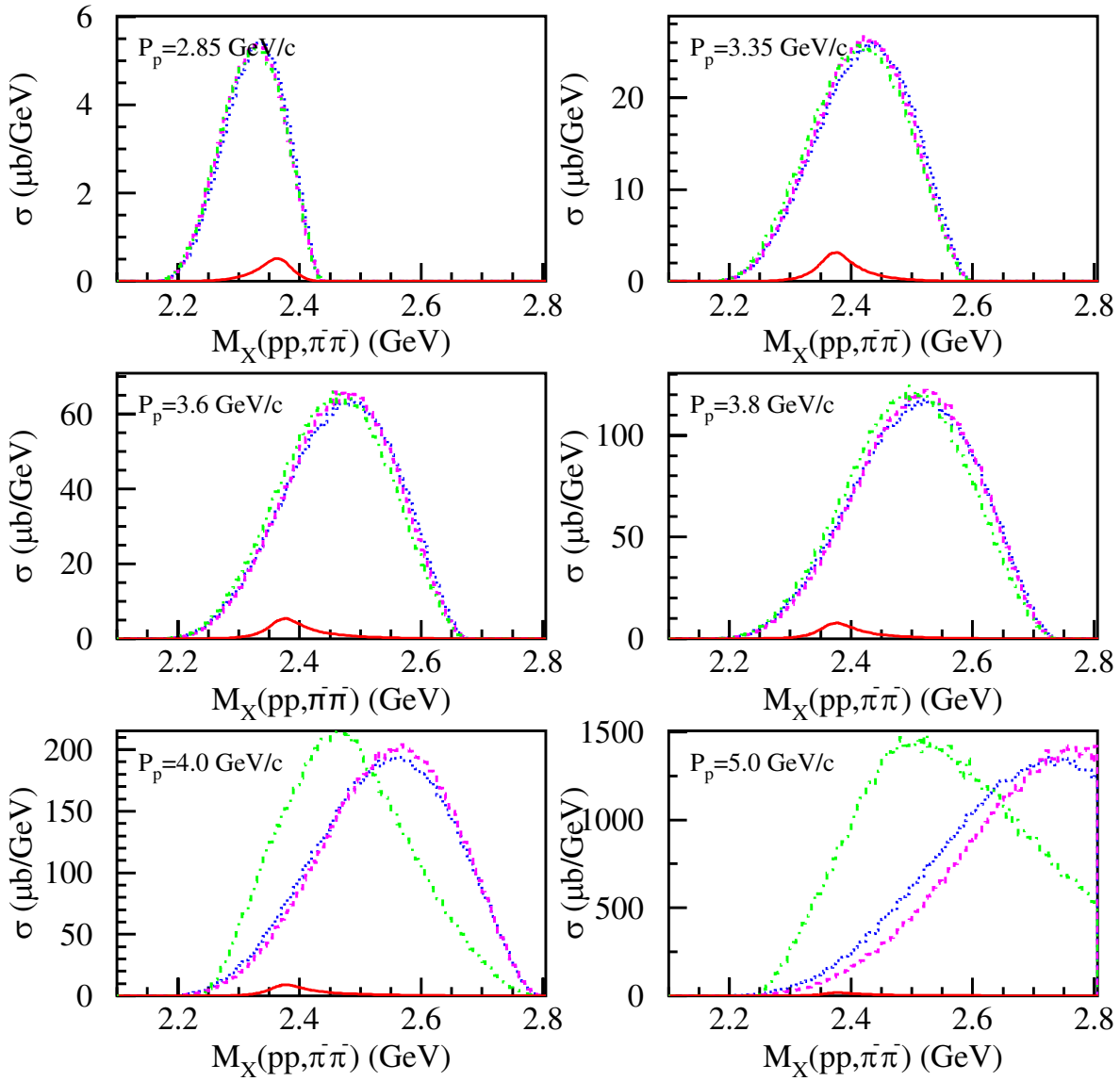

FIG. 11. Missing mass M_X distributions for the $pp \to \pi^-\pi^- X$ reaction at the incident proton momentum of 2.85, 3.35, 3.6, 3.8, 4.0, and 5.0 GeV/c. The dotted curve (blue) shows the background $pp \to \pi^+\pi^+\pi^-\pi^- pp$ contribution, The dashed curve (magenta) shows the two-Roper-resonance contribution, the dotted-dashed curve (green) shows the two-$N(1520)D_{13}$ contribution, and the solid curve (red) shows the $pp \to \pi^-\pi^-\mathcal{D}_{30}^{++++}$ contribution.

mass distributions for the $pp \to \pi^-\pi^- X$ reaction at the incident proton momentum of 3.6, 3.8, 4.0, and 5.0 GeV/c. In this plot, the pure phase-space contributions and the two-Roper-resonance-production contributions are very similar, but the latter contributions are slightly shifted to the lower side especially for the higher incident momenta. The two-$N(1520)D_{13}$-

production contributions with a mass of 1.52 GeV and width of 0.11 GeV for $N(1520)D_{13}$ are also plotted in Fig. 11, and they are very similar to the pure phase-space contributions at lower incident momenta. Sizable deviations are observed at incident momenta higher than 3.8 GeV/c. It is important to measure cross sections at several incident momenta for studying the background.

A signal-to-noise (S/N) ratio is not so high even at 3.35–3.60 GeV/c, the optimum incident momentum of the proton beam. Here, the possibility of background reduction is briefly discussed. An isoscalar dibaryon $\mathcal{D}_{03}$ dominantly decays into $\pi\mathcal{D}_{12}$ with a mass of ~ 2.15 GeV and width of ~ 0.09 GeV, and $\mathcal{D}_{12}$ is successively de-excited into the deuteron emitting π. Analogously, a possible decay chain of $\mathcal{D}_{30}^{++++}$ is considered as $\mathcal{D}_{30}^{++++} \to \pi^+\mathcal{D}_{21}^{+++} \to \pi^+\pi^{+2}$He, where ^{2}He stands for a diproton state, or a nucleus of an extremely unstable isotope of helium without any neutrons. Fig. 12 shows the decay chain of $\mathcal{D}_{03}$ and possible decay chain of $\mathcal{D}_{30}$. The correlation may help for $\mathcal{D}_{30}$ identification between the π^+pp invariant mass and the missing mass for the $pp \to \pi^-\pi^-X$ reaction (equivalent to the $\pi^+\pi^+pp$ invariant mass). The ^{2}He formation between two protons may also lead to $\mathcal{D}_{30}$ identification.

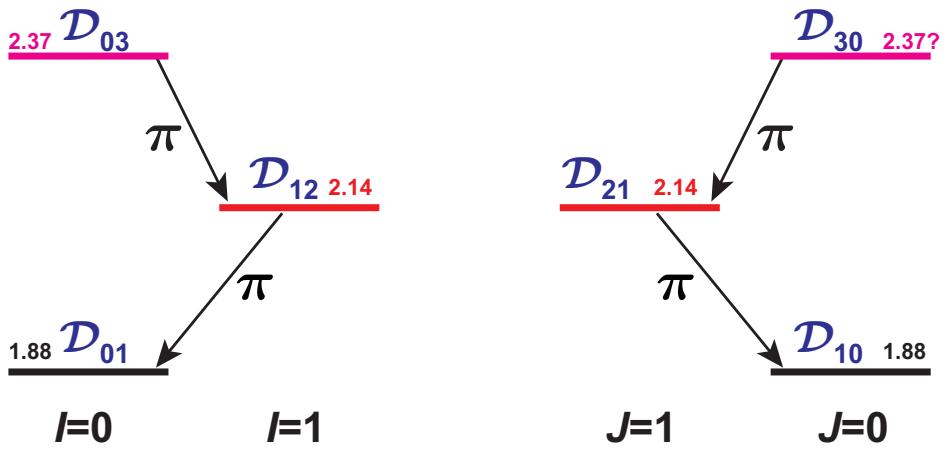

FIG. 12. Decay chain of $\mathcal{D}_{03}$ (left) and possible decay chain of $\mathcal{D}_{30}$ (right). Since the $\mathcal{D}_{03} \to \pi\mathcal{D}_{12} \to \pi\pi d$ decay is observed, the $\mathcal{D}_{30} \to \pi\mathcal{D}_{21} \to \pi\pi\,(NN)_{J=0}$ ($\mathcal{D}_{30}^{++++} \to \pi^+\mathcal{D}_{21}^{+++} \to \pi^+\pi^{+2}$He) decay is expected in the mirrored quantum-number states.

III. EXPERIMENTAL SETUP

We use the general-purpose E50 detector system for this experiment. The E50 experiment at J-PARC performs charmed-baryon spectroscopy by means of a missing-mass measurement for the $\pi^- p \to D^{*-} X$ reaction at the high-intensity high-momentum secondary beamline [41–49]. The excitation spectrum of charmed baryons would reveal diquark correlation as a possible effective degree of freedom for describing hadrons. Unseparated secondary beam with a negatively charged particles is provided in the main E50 experiment. In the present experiment, we use the proton beam, and positively-charged particles are provided onto the target. The target used is a liquid hydrogen with a thickness of 570 mm, corresponding to 2.58 b^{-1}.

The momentum analysis of produced charged particles is made with a large-acceptance magnetic dipole spectrometer. Fig. 13 shows the current version of the planned E50 spectrometer. It consists of a dipole magnet, which was a magnet for a frequency-modulated (FM) cyclotron at the Institute of Nuclear Study (INS), University of Tokyo, and detectors for tracking, time-of-flight measurement, and particle identification. The magnet has a circular pole with a diameter of 2.12 m and a gap of 1 m. An integrated magnetic field flux of 2.3 T·m is expected at maximum. Finely-segmented scintillating fiber hodoscopes are employed for upstream tracking detectors, located surrounding the target. High-granularity drift chambers are laid out downstream of these hodoscopes for measuring trajectories of charged particles. To provide a reference timing, an acrylic Cherenkov hodoscope is placed just in front of the target. Resistive-plate chambers are placed behind the drift chambers for time-of-flight measurement, giving a mass of charged particles together with its momentum, and flight length. Threshold-type Cherenkov detectors and a ring-imaging Cherenkov detector are laid out in the most downstream side. Detected are pions and protons with momenta higher than 0.1 and 0.5 GeV/c, respectively.

The intensity of each particle in the secondary beam is estimated by using the Sanford-Wang formula [50–52]. Here, we assume a platinum target for production of secondary particles with a production angle of 2.5° with the so-called beam swinger optics [53], and a 15-kW loss of the primary beam at the target. Additionally, the in-flight decay of charged particles is taken into account for traveling a length of 132 m, and the estimated momentum and angular bite of the beamline of 2 msr·% is also incorporated. Fig. 14 shows the

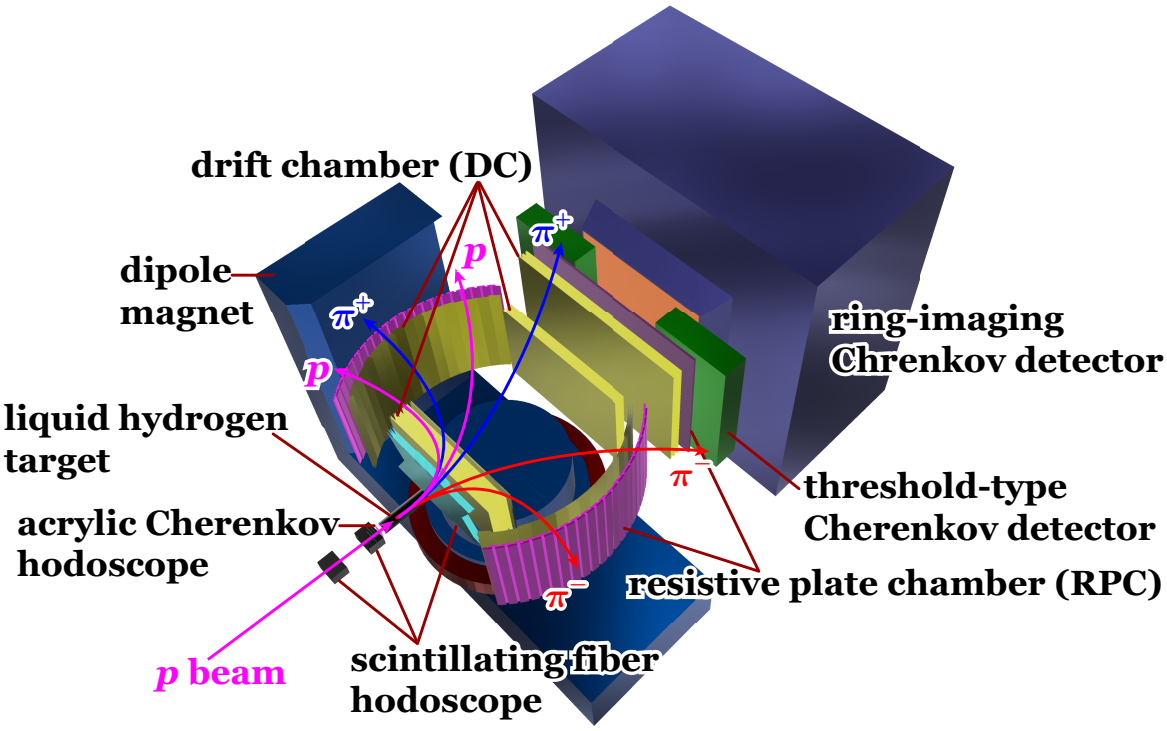

FIG. 13. Current design of the planned E50 spectrometer. It consists of a dipole magnet, tracking detectors, and time-of-flight detectors. The target used is liquid hydrogen with a thickness of 570 mm. Finely-segmented scintillating fiber hodoscopes are employed for upstream tracking detectors, located in front of and behind the target, and drift chambers are placed downstream. Resistive-plate chambers are placed behind the drift chambers for the time-of-flight measurement. To provide a reference timing, an acrylic Cherenkov hodoscope is just in front of the target. Threshold-type Cherenkov detectors and a ring-imaging Cherenkov detector are placed at most downstream.

estimated beam intensity as a function of the beam momentum for the 15-kW loss. At a momentum of 3.8 GeV/c, 40-MHz pions and 20-MHz protons are expected to be provided. Table III summarizes the maximum intensity of protons, positive pions, and positive kaons at momenta of 2.85, 3.35, 3.6, 3.8, and 4.0 GeV/c. It should be noted that the secondary beam extraction is made for the 2-s duration of every 5.2 s cycle, giving the duty factor is 0.385.

Since the secondary beam used is unseparated, the protons among the beam have to be tagged by a beamline Cherenkov detector placed on the beamline at the most upstream (not shown in Fig. 13). The detector, which is now under development in the E50 collaboration,

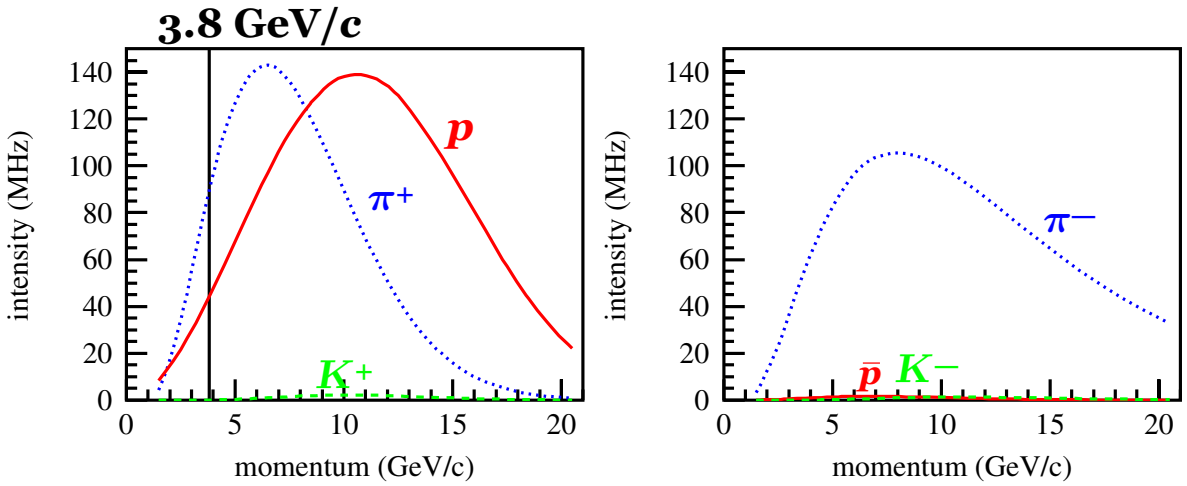

FIG. 14. Maximum intensity of charged particles in a secondary beam as a function of the momentum. The left and right panels show those for positively and negatively charged particles, respectively. A momentum of 3.8 GeV/c gives a secondary beam containing approximately 107-MHz positive pions and 53.7-MHz protons. The solid curves (red) show protons and anti protons, the dotted (blue) present pions, and the dashed (green) indicate kaons.

TABLE III. Maximum intensity of protons, positive pions, and positive kaons at momenta of 2.85, 3.35, 3.6, 3.8, and 4.0 GeV/c. The secondary beam is extracted for the 2-s duration of every 6-s cycle, giving the duty factor is 0.385.

incident momentum (GeV/c)	2.85	3.35	3.6	3.8	4.0
proton intensity (MHz)	35.7	45.0	49.8	53.7	57.6
positive pion intensity (MHz)	70.4	90.9	100	107	114
positive kaon intensity (kHz)	23.7	70.2	108	146	192

is planned to separate charged particles by means of Cherenkov ring measurement. The observed Cherenkov ring will separated pions, kaons, and protons upto a few tens of MHz in this detector. Even if we cannot use it, we can alternatively use a threshold-type Cherenkov detector with a refractive index of 1.03 up to a few MHz. In the following section, a secondary beam containing 2-MHz positive pions, and 1-MHz protons is considered for yield estimations. The high-intensity high-momentum secondary beamline is expected to be constructed step by step. Since this requirement for the beam intensity corresponds to

the 0.5-kW loss (1/30 of the final goal) of the primary beam at the production target, the proposed experiment can be performed before the main E50 experiment becomes ready.

We plan to use a trigger-less streaming DAQ system [54] for the E50 experiment. This allows us to make the DAQ efficiency close to 100% without any trigger bias. However, we make yield estimations using a conservative DAQ efficiency assuming to use an ordinary DAQ system in §IV.

IV. YIELD ESTIMATIONS

We use proton beams with momenta around 3.0–4.0 GeV/c, and have estimated the differential cross sections at a mass of 2.38 GeV for $\mathcal{D}_{30}^{++++}$ production and background contribution as already discussed in the previous section. The total cross sections are assumed to be proportional to three-body and six-body pure-phase contributions for $\mathcal{D}_{30}$ production ($pp \to \pi^-\pi^-\mathcal{D}_{30}^{++++}$) and background ($pp \to \pi^-\pi^-\pi^+\pi^+pp$), and they are normalized to those measured by the WASA-at-COSY collaboration at $T_p = 2.063$ and 2.541 GeV. Table IV summarizes the numerical values for the estimated differential cross sections at a mass of 2.38 GeV/c for $\mathcal{D}_{30}$ production and background phase-space contribution.

TABLE IV. Estimated differential cross sections at a mass of 2.38 GeV for $\mathcal{D}_{30}$ production and background. We assume the energy dependences of the total cross sections are proportional to three-body and six-body pure-phase contributions for $\mathcal{D}_{30}$ production ($pp \to \pi^-\pi^-\mathcal{D}_{30}^{++++}$) and background ($pp \to \pi^-\pi^-\pi^+\pi^+pp$), respectively. They are normalized to those measured by the WASA-at-COSY collaboration at $T_p = 2.063$ and 2.541 GeV.

incident momentum (GeV/c)	2.85	3.35	3.60	3.80	4.00
$\mathcal{D}_{30}$ production (μb/GeV)	0.43	3.1	5.4	7.8	9.2
phase-space background (μb/GeV)	3.9	21	40	57	75

Detecting two negative pions are the most important in this experiment. At first, we estimate the momentum distributions of them. Fig. 15 shows the momentum distributions of negative pions produced in the $pp \to \pi^-\pi^-\pi^+\pi^+pp$ and $pp \to \pi^-\pi^-\mathcal{D}_{30}^{++++}$ reactions. The momenta of negative pions range from 0 to 1.4 GeV/c, and events with higher-momentum

negative pions are relatively enhanced in the $pp \to \pi^-\pi^-\mathcal{D}_{30}^{++++}$ reaction at higher incident momenta of the proton beam. This is because the mass of $\mathcal{D}_{30}^{++++}$ is located in the lower M_X region. Since a fraction of very slow negative pions are small, almost all the pions can be detected if they are emitted within the solid angle of the E50 spectrometer.

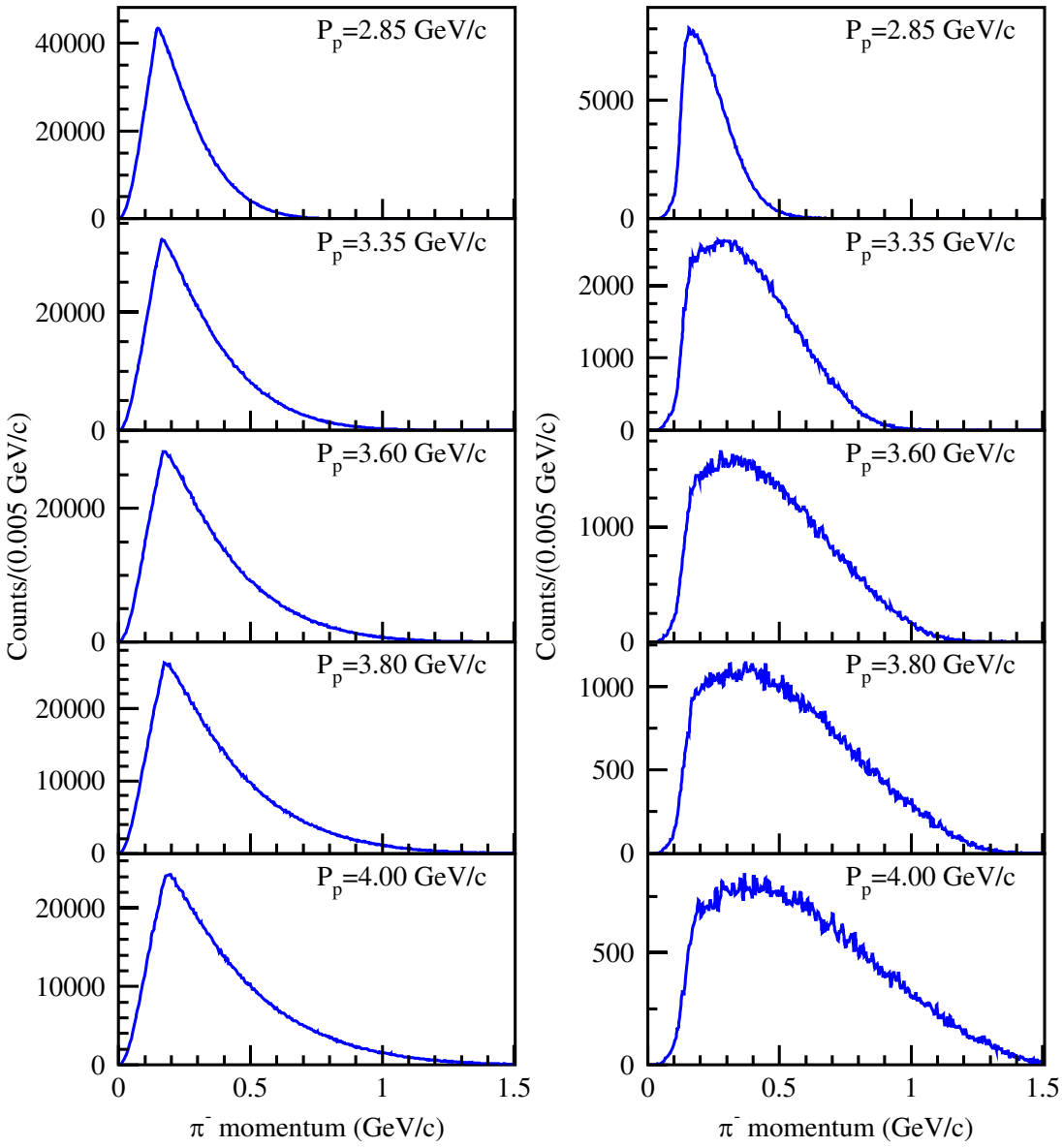

FIG. 15. Momentum distribution of negative pions produced in the $pp \to \pi^-\pi^-\pi^+\pi^+pp$ reaction (left), and in the $pp \to \pi^-\pi^-\mathcal{D}_{30}^{++++}$ reaction (right).

We also estimate the angular distributions of pion and proton emission. Owing to high incident momenta of the proton beam, most of the produced particles are emitted at forward angles. Fig. 16 shows the angular distributions of pion and proton emission produced in the

$pp \to \pi^-\pi^-\pi^+\pi^+pp$ reaction. Almost all the protons are emitted at the forward angles less than 30°, pions are also emitted at forward angles less than 60°.

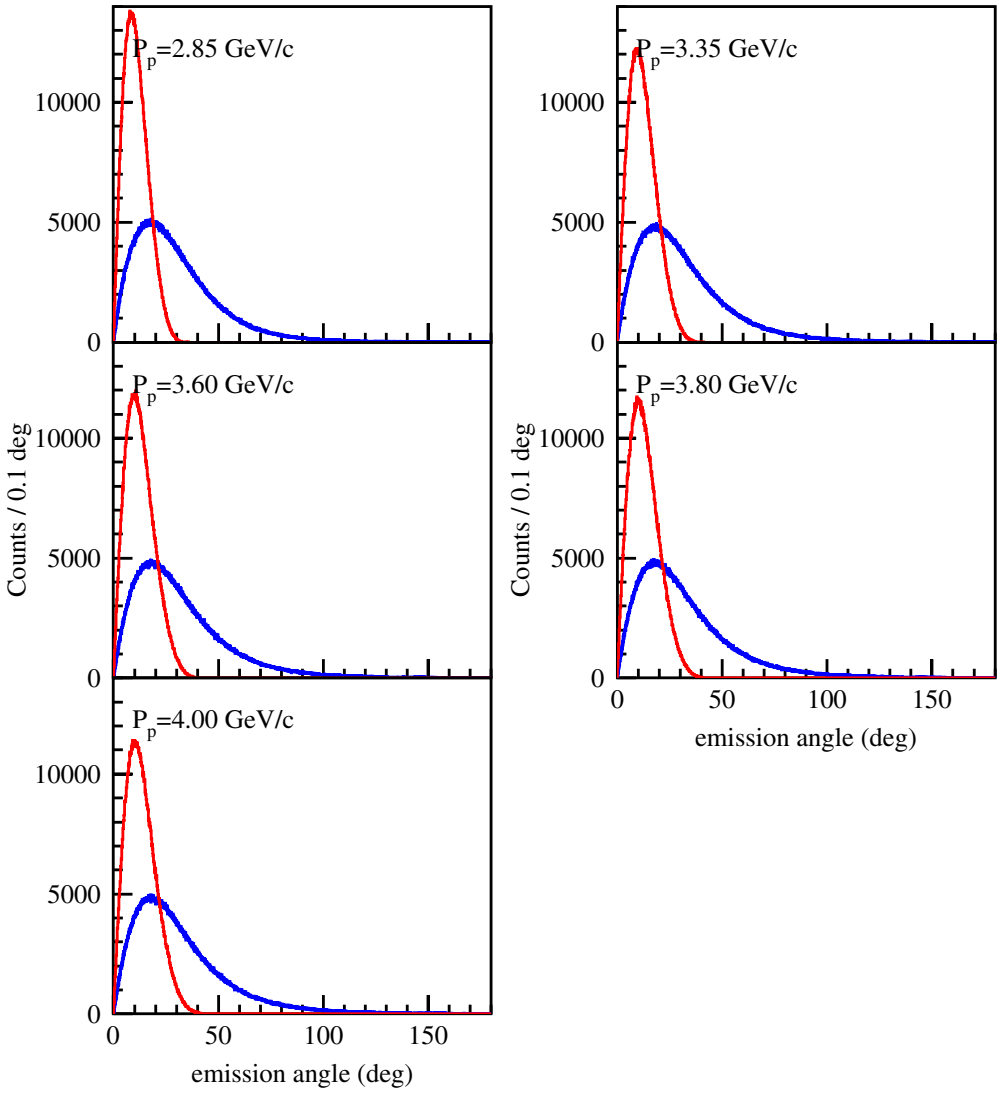

FIG. 16. Angular distributions of pions (blue) and protons (red) produced in the $pp \to \pi^-\pi^-\pi^+\pi^+pp$ reaction. Almost all the protons are emitted at forward angles less than 30°, pions are also emitted at forward angles less than 60°.

Now, we consider the reason for poor acceptance for identifying the $pp \to \pi^-\pi^-\pi^+\pi^+pp$ reaction including particle identification in the previous WASA-at-COSY experiment. In Ref. [34], the acceptances are only 0.1% and 0.5% for detecting $\pi^-\pi^-\pi^+\pi^+pp$ at $T_p = 2.063$ and 2.541 GeV, respectively. The forward detector in WASA covers 3°–17°, and the central covers 20°–170° [55]. Fig. 17 shows the correlation plot between the number of detected charged particles in the forward and central detectors. The correlations are estimated for

the pure phase-space generation of the final state particles. The angular distributions of pion emission must distort these correlations somehow. The trigger condition was required that more than one charged particles were detected in each of the forward and central detectors in WASA. As shown in Fig. 17, this condition did not decrease the acceptance so much. Since charge identification and momentum determination with a magnetic field were available only for the central detector, they required that the two protons were detected with the forward detector, and that the other charged pions were detected with the central detector. This condition gave the geometrical acceptances of approximately 10% (more or less depending on the angular distributions of pions) for detecting $\pi^-\pi^-\pi^+\pi^+pp$, but the final acceptances are only 0.1% and 0.5% at $T_p = 2.063$ and 2.541 GeV, respectively.

These discrepancies come from a poor particle-identification power in the WASA detector [59]. The forward detector in WASA is a range-stack counter consisting of plastic scintillators, and reliable particle identification is difficult for many events owing to the hadronic interaction in the detector material. The particle-identification efficiency including the tracking efficiency for pions is also low in the central detector owing to many e^+e^- tracks converted from photons. At $T_p = 2.541$ GeV, the additional missing-mass trigger, which we don't know in detail, may also decrease the acceptance. Thanks to high capability of particle identification with the E50 spectrometer, the total acceptance can be reliably estimated and increased much higher than WASA.

Next, the geometrical acceptance of the E50 spectrometer is estimated for $\pi^-\pi^-$ detection by using a Monte-Carlo simulation based on Geant4 [56–58]. Fig. 18 shows the M_X distributions for the $pp \to \pi^-\pi^- X$ reaction, and acceptances as a function of M_X. The acceptance gradually increases with increase of the missing mass M_X for the $pp \to \pi^-\pi^- X$ reaction, and is approximately 0.38 at $M_X \simeq 2.38$ GeV almost independently of the incident proton momentum. The variation of the acceptance is very small with a change of M_X except the highest M_X region where negative pions are likely to be emitted backward angles, and their momenta are low.

Here, the yield in a 0.01-GeV-M_X bin is considered for $\pi^-\pi^-$-detected events at $M_X = 2.38$ GeV. The estimated differential cross sections for $\mathcal{D}_{30}$ production at 2.38 GeV together with those for the background contribution are listed in Table IV. We assume that the thickness of the target is 2.58 b^{-1}, that the geometrical acceptance of the E50 spectrometer is 0.38, that the beam intensity is 1 MHz, and that the duty factor is 0.385. The expected

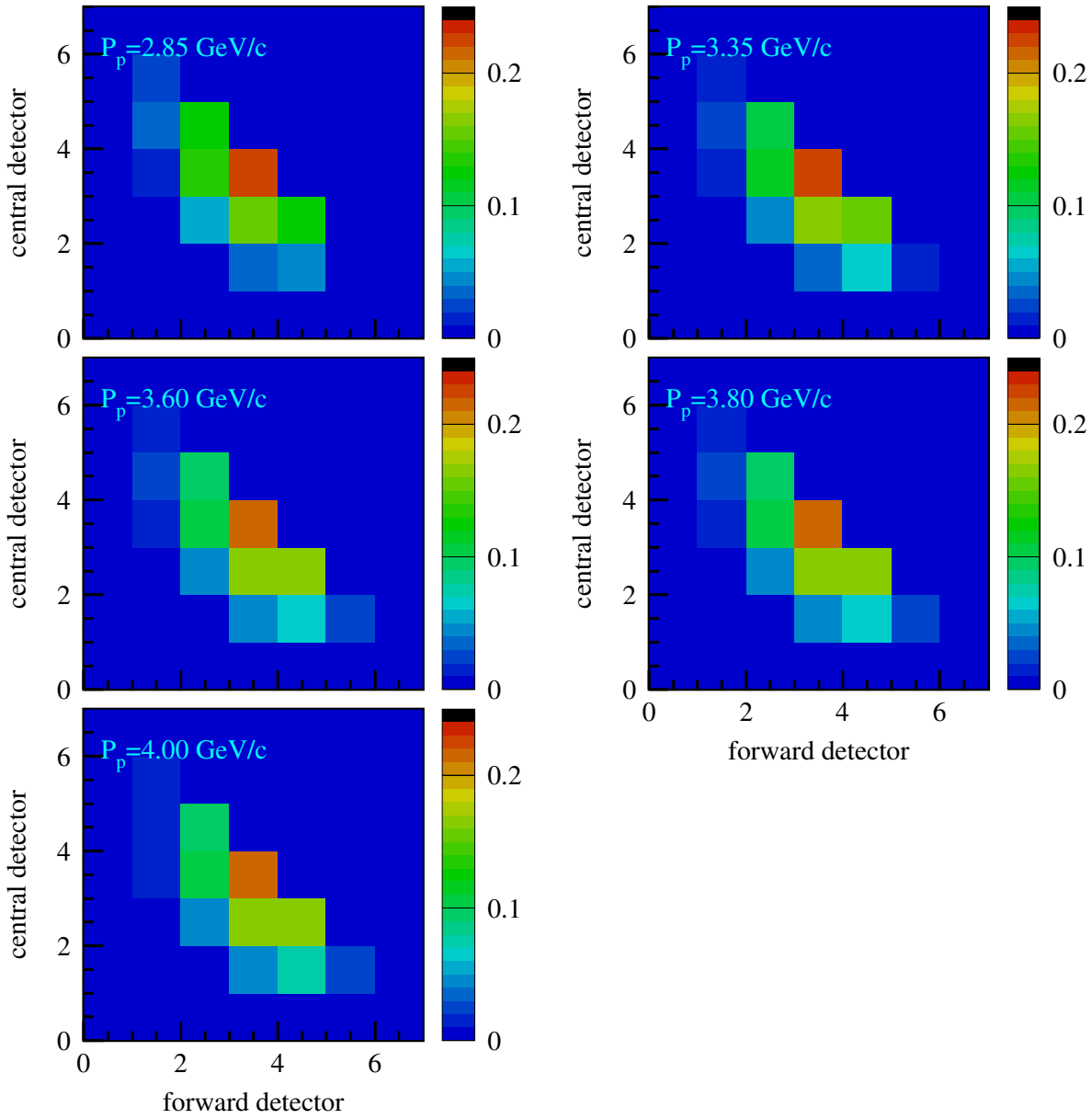

FIG. 17. Correlation plot between the number of detected charged particles in the forward and central detectors. The forward detector denotes the polar angles of 3°–17°, and the central denotes those of 20°–170° [55].

numbers of $\pi^-\pi^-$-detected $\mathcal{D}_{30}^{++++}$-produced events within a 0.01-GeV-M_X bin at 2.38 GeV for a one-day measurement are summarized in Table V together with their statistical uncertainties (including the background subtraction).

Although $\pi^-\pi^-$ detection is the minimum requirement in this experiment, it is very important to detect all the final-state particles to study the decay of $\mathcal{D}_{30}^{++++}$ and possi-

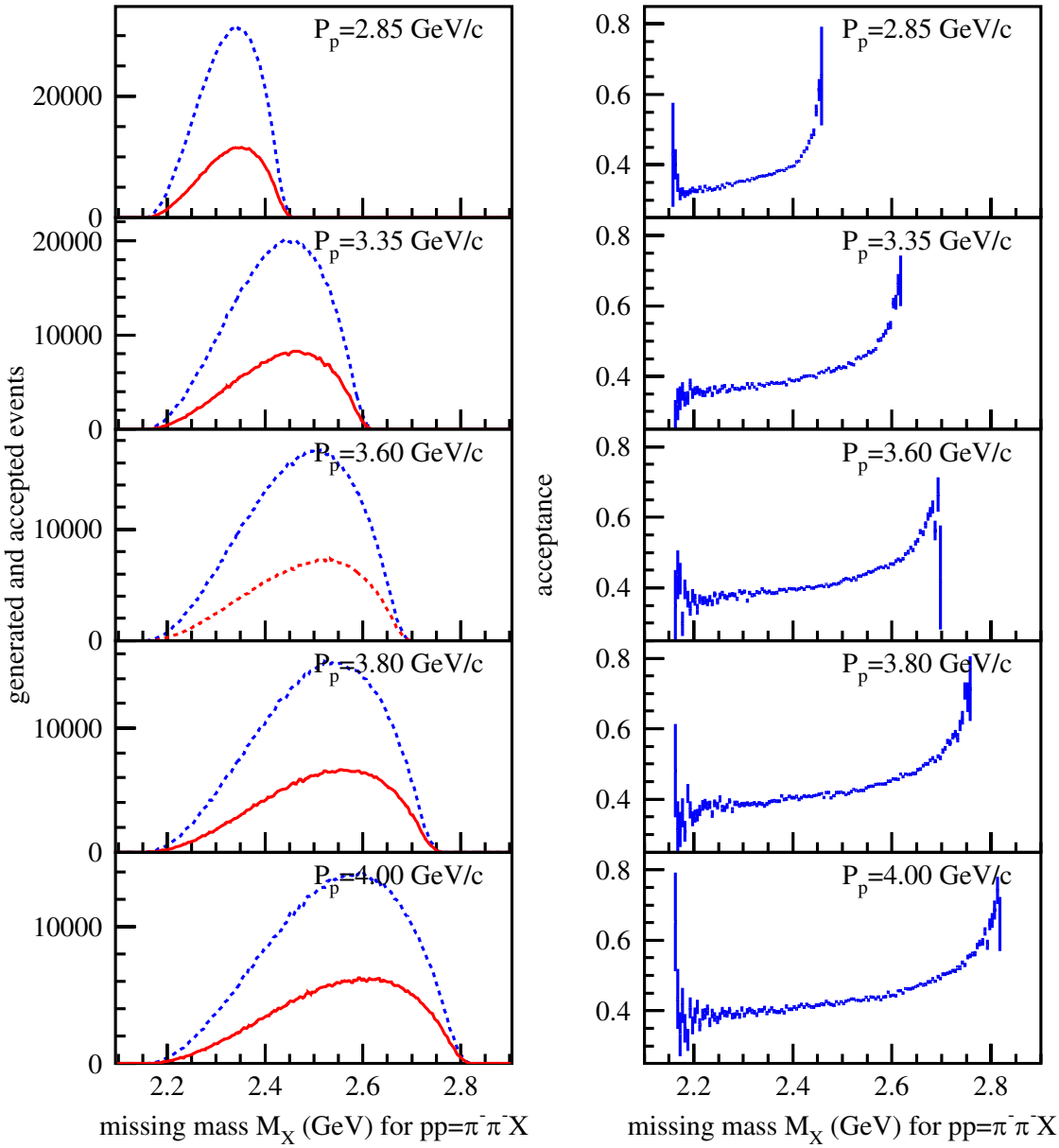

FIG. 18. Missing mass M_X distributions for the $pp \to \pi^-\pi^- X$ reaction (left), and geometrical acceptances as a function of M_X (right). In the left panel, the dotted histogram (blue) is the M_X distribution for the generated events (regardless of particle detection), and the solid one (red) is that for the accepted events (both the two negative pions are detected).

ble background reduction. Small background contributions with additional pions, $pp \to (\pi^-\pi^-\pi^+\pi^+pp)\pi^0$, $pp \to (\pi^-\pi^-\pi^+\pi^+pp)\pi^+\pi^-$, and $pp \to (\pi^-\pi^-\pi^+\pi^+pp)\pi^0\pi^0$, can be removed by using the energy and momentum conservation between the initial and final states. We also estimate the efficiencies of $\pi^-\pi^-\pi^+$, $\pi^-\pi^-\pi^+\pi^+$, and $\pi^-\pi^-\pi^+\pi^+pp$ detections.

TABLE V. Estimated numbers of $\pi^-\pi^-$-detected events at a mass of 2.375–2.385 GeV/c for a one-day measurement. Here, we assume a 100% tracking and particle-identification efficiencies. The statistical uncertainties include the background subtraction effects.

incident momentum (GeV/c)	2.85	3.35	3.60	3.80	4.00
expected yield	121	875	1530	2200	2600
statistical uncertainty (%)	29	9.4	7.4	6.1	5.9

Fig. 19 shows these efficiencies together with those of $\pi^-\pi^-$ detection. The efficiency of $\pi^-\pi^-\pi^+\pi^+pp$ detection is 0.4 times as high as that of $\pi^-\pi^-$ detection. Thanks to the large solid angle of the E50 spectrometer, the efficiency drop is not serious even if we require to detect all the final-state particles. And no significant difference of the efficiencies is observed between $\pi^-\pi^-\pi^+\pi^+$ and $\pi^-\pi^-\pi^+\pi^+pp$ detections.

Again, the yield in a 0.01-GeV-M_X bin is considered for $\pi^-\pi^-\pi^+\pi^+pp$-detected events at $M_X = 2.38$ GeV. Only the geometrical acceptances are modified from the yield estimation of the $\pi^-\pi^-$-detected events. Although the efficiencies of $\pi^-\pi^-$ detection are approximately 0.38 at $M_X = 2.38$ GeV independently of the incident momentum of the proton beam, those of $\pi^-\pi^-\pi^+\pi^+pp$ detection are 0.13, 0.16, 0.16, 0.17, and 0.18 for incident momenta of 2.85, 3.35, 3.60, 3.80, and 4.00 GeV/c, respectively. The negative pions are likely to be emitted at more forward angles (although this effect is small and it is difficult to observe in Fig. 16), resulting in the higher geometrical acceptance, for the higher incident momenta. The expected events of $\mathcal{D}_{30}^{++++}$ production with their statistical uncertainties for a one-day measurement are summarized in Table VI.

TABLE VI. Estimated numbers of $\pi^-\pi^-\pi^+\pi^+pp$-detected events at a mass of 2.375–2.385 GeV/c for a one-day measurement. Here, we assume a 100% tracking and particle-identification efficiencies.

incident momentum (GeV/c)	2.85	3.35	3.60	3.80	4.00
expected yield	40.9	357	618	985	1240
statistical uncertainty (%)	49.6	14.8	11.7	9.2	8.6

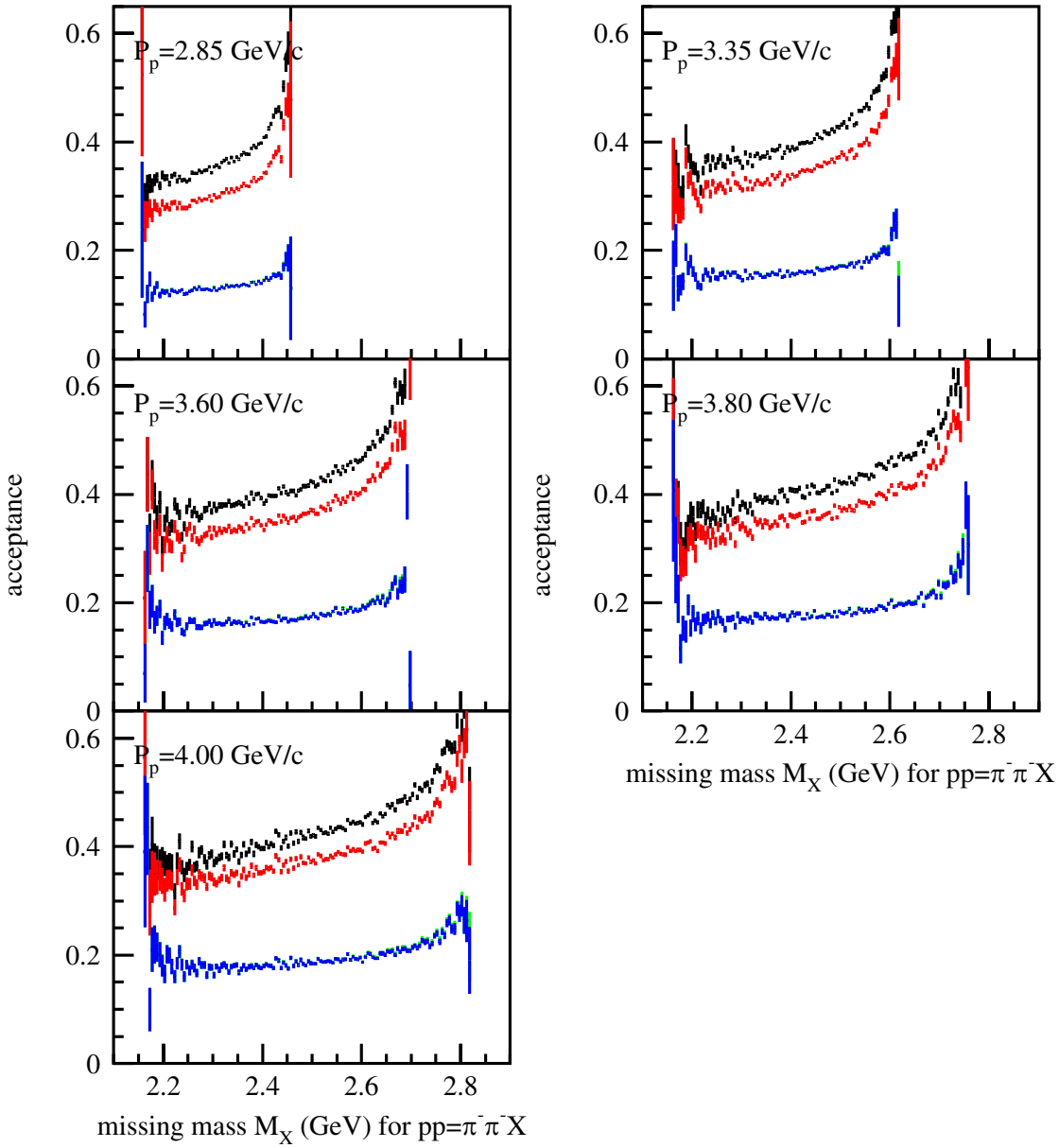

FIG. 19. Geometrical acceptances of $\pi^-\pi^-$ (black), $\pi^-\pi^-\pi^+$ (red), $\pi^-\pi^-\pi^+\pi^+$ (green), and $\pi^-\pi^-\pi^+\pi^+pp$ (blue) detections as a function of M_X for the $pp \to \pi^-\pi^- X$ reaction. The efficiencies are estimated for the pure six-body phase-space $\pi^-\pi^-\pi^+\pi^+pp$ events. No significant difference of the efficiencies is observed between $\pi^-\pi^-\pi^+\pi^+$ (green) and $\pi^-\pi^-\pi^+\pi^+pp$ (blue) detections.

Thus far, the geometrical acceptances are estimated by assuming a 100% DAQ, tracking and particle-identification efficiencies. We estimate the expected yield with some realistic assumptions for the DAQ, tracking, and particle identification efficiencies. We plan to use

a trigger-less streaming DAQ system for the E50 experiment [54]. This allows us to make the DAQ efficiency close to 100% without any trigger bias. Here, the conservative DAQ efficiency is estimated. The total cross section is assumed to be 1 mb for the reactions with more than five final-state particles (0.4 mb for $pp \to \pi^-\pi^-\pi^+\pi^+pp$ at 4.0 GeV/c). The 3-MHz unseparated secondary beam gives the trigger rate of 1.2 kHz taking into account an approximate 15% acceptance. Assuming the dead time for processing an event is 25 μs, the DAQ efficiency is higher than 0.97. The tracking efficiency assumed is 0.90 for each track, resulting in the total tracking efficiency of 0.53 for six-track events. The efficiency of particle identification assumed is 0.95 for each track, giving 0.73 for the total particle identification. The tracking and particle identification efficiency of the secondary beam is assumed to be 0.90. Then, the total efficiency of the event reconstruction is assumed to be higher than 0.34 for all the incident momenta. This efficiency of 0.34 for the total event reconstruction is applied in the following yield estimations.

Finally, we estimate the statistical uncertainties for the mass and width determination of $\mathcal{D}_{30}^{++++}$. Fig. 20 shows the typical missing mass M_X distributions for the $pp \to \pi^-\pi^-\pi^+\pi^+pp$ reactions at 2.85, 3.35, 3.60, 3.80, and 4.00 GeV/c. These distributions are estimated assuming the three-day measurement for all the incident momenta. The number of events are obtained according to the estimated total cross sections for $\mathcal{D}_{30}^{++++}$ production and background phase-space contribution, and the acceptance of the E50 spectrometer is taken into account. Since the signal-to-noise (S/N) ratio is not so high, the $\mathcal{D}_{30}^{++++}$ contribution is not observed as a peak but a shoulder. To deduce the mass and width of $\mathcal{D}_{30}^{++++}$ from each distribution, we fit a function expressed by a sum of the $\mathcal{D}_{30}$ production with a different mass and a different width, and a different strength background phase-space contribution. The extracted $\mathcal{D}_{30}^{++++}$ contribution is also plotted in Fig. 20, which is obtained by subtracting a background contribution from a measured distribution. The $\mathcal{D}_{30}^{++++}$ contribution has been correctly obtained. When the amounts of the signal (S) and noise (N) are obtained as the number of events for masses ranging from 2.25 to 2.45 GeV, the S/N ratios are 0.104, 0.097, 0.088, 0.089, and 0.079 at 2.85, 3.35, 3.60, 3.80, and 4.00 GeV/c, respectively.

To get the beamtime for determining the mass and width of $\mathcal{D}_{30}^{++++}$ precisely for each incident proton momentum, we modify the duration of the measurement and estimate the statistical uncertainty of the determined mass and width. Fig. 21 shows the expected statistical uncertainties for the mass and width for $\mathcal{D}_{30}^{++++}$ as a function of the number of days for

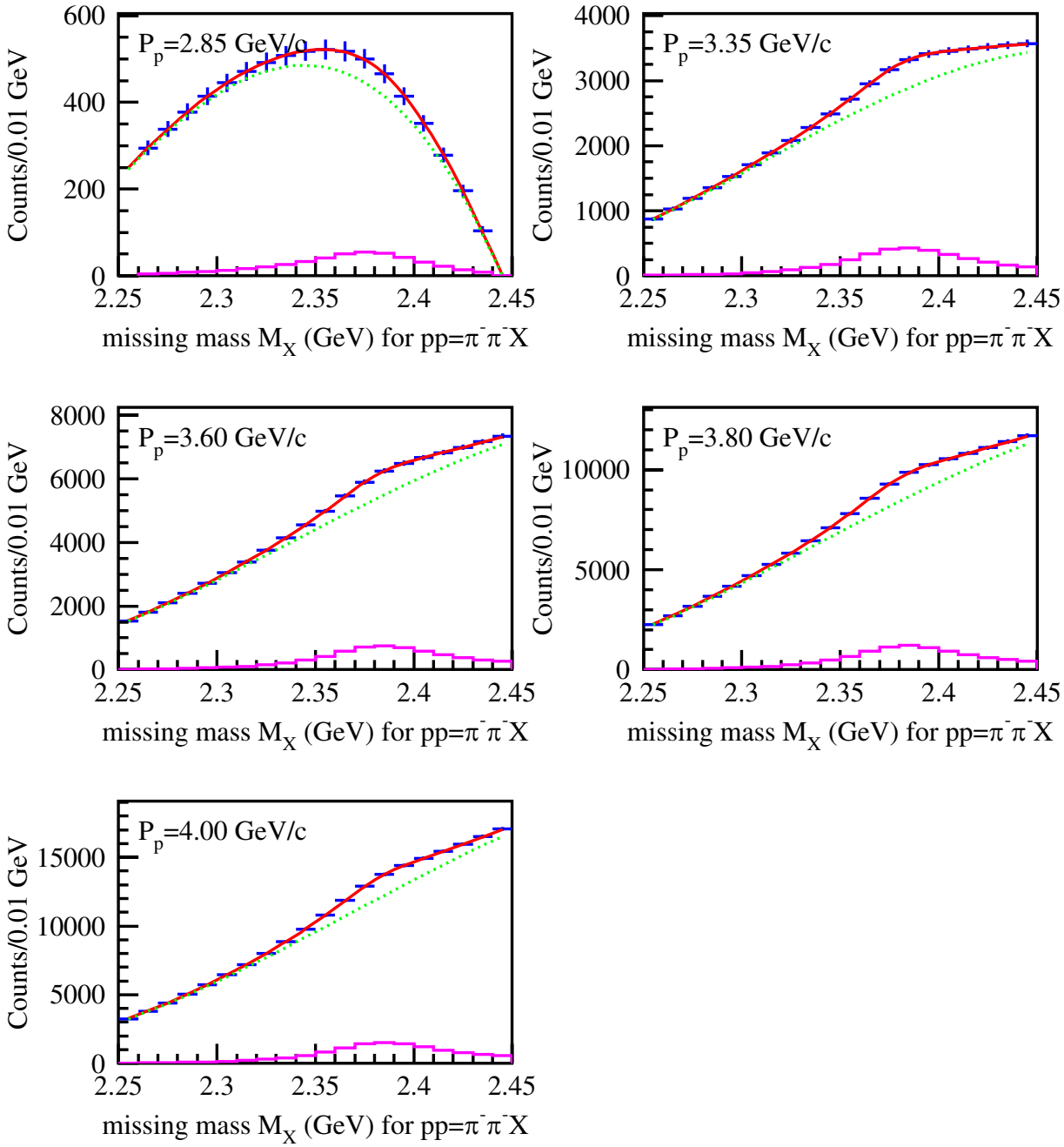

FIG. 20. Missing mass M_X distributions for the $pp \to \pi^-\pi^-\pi^+\pi^+pp$ reactions at 2.85, 3.35, 3.60, 3.80, and 4.00 GeV/c. The markers correspond to the expected experimental data obtained in a three-day measurement for all the incident momenta. In each panel, the solid curve (red) shows the fitted function expressed by a sum of the $\mathcal{D}_{30}$ production and background phase-space contribution. The histogram (magenta) represents the extracted $\mathcal{D}_{30}$ contribution, and the dotted curve (green) shows the background contribution.

each incident proton momentum. We need more days to get the same precision of the width determination at lowest incident proton momenta of 2.85 GeV/c where the WASA-at-COSY collaboration tried to search for $\mathcal{D}_{30}$. This is partly because the total cross sections are not so high for this momentum, and partly because the peak positions are not clearly separated between $\mathcal{D}_{30}^{++++}$ production and background phase-space contributions. We request three days for each measurement to confirm the existence of $\mathcal{D}_{30}^{++++}$ and determine the total cross

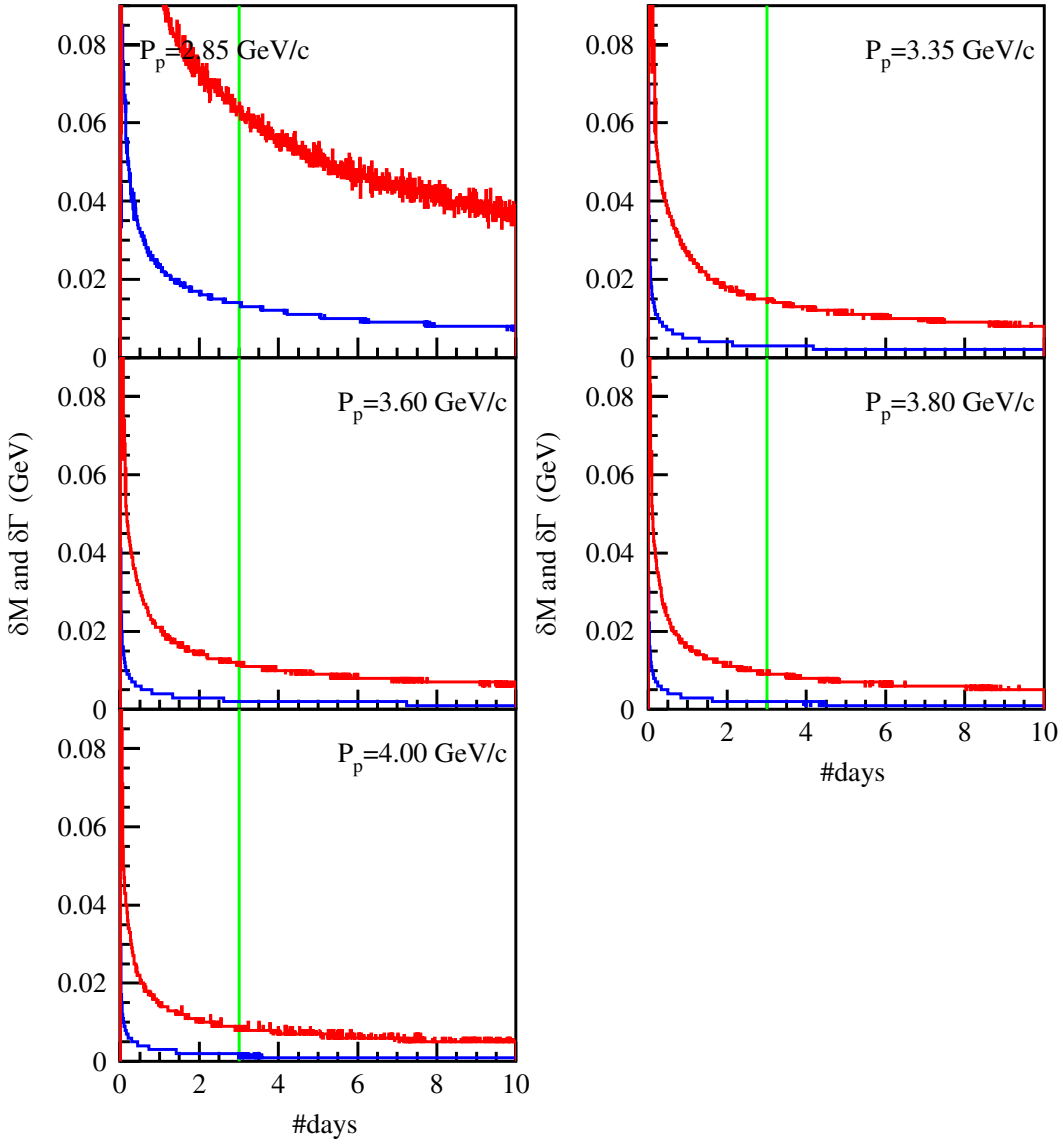

FIG. 21. Expected statistical uncertainties for the mass (M) and width (Γ) for $\mathcal{D}_{30}^{++++}$ as a function of the number of days for each incident proton momentum. The blue and red curves represent the statistical uncertainty for M and Γ, respectively.

section of $\mathcal{D}_{30}^{++++}$ production. As for the incident momentum of 2.85 GeV/c, we only aim at checking a consistency with the WASA-at-COSY results. The estimated statistical uncertainties are 0.003, 0.002, 0.002, and 0.002 GeV for the mass determination at incident momenta of 3.35, 3.60, 3.80, and 4.00 GeV/c, respectively. While those for the width are 0.015, 0.011, 0.009, and 0.009 GeV/c, respectively. Combining all the data acquired, the estimated statistical uncertainties become 0.001 and 0.004 GeV for the mass and width, respectively.

A possible improvement of the S/N ratio is discussed below. It was very important to detect the deuteron in the final state when the CELSIUS/WASA collaboration got a clear evidence of $d^*(2380)$ for the first time. The deuteron identification was considered to suppress a huge background contribution, and the branching ratios of $d^*(2380)$ are enough high as $14\% \pm 1\%$ and $23 \pm 2\%$ for the $\pi^0\pi^0 d$ and $\pi^+\pi^- d$ final states, respectively [60]. In analogy to this situation, $\mathcal{D}_{30}$ can be likely to decay into $\pi^+\pi^+{}^2$He as shown in Fig. 12, and the ^{2}He identification is expected to suppress the background. Since the ^{2}He nucleus is a scattering state of the two protons, the mass distribution is calculated using a Migdal-Watson formula [61–63]:

$$|T|^2 = \left(\frac{\sin\delta}{k}\right)^2 \exp\left(-2\pi\eta\right), \tag{2}$$

where k denotes the proton momentum in the CM frame, and $\exp\left(-2\pi\eta\right)$ stands for the Coulomb penetration factor evaluated at $\eta = \alpha m_p/2k$. The $\delta(k)$ is the combined Coulomb-nuclear phase shift. For obtaining the mass distribution, we simply employ the S-wave nuclear phase shift for it from the scattering parameters (the scattering length of $a_{pp} = -17.3$ fm and an effective range of $r_{pp} = 2.85$ fm [64]). Fig. 22 shows the mass distribution of the ^{2}He nucleus (the diproton state).

Here, ^{2}He is identified by requiring that the pp invariant mass is less than 1.88 GeV, giving a ^{2}He-tagging efficiency of 0.41. The background contributions are reduced by a factor of 1/30.0, 1/32.3, 1/33.6, 1/40.2, and 1/33.9 at incident momenta of 2.85, 3.35, 3.60, 3.80, and 4.00 GeV/c, respectively. Fig. 23 shows the pp invariant-mass distributions for the $pp \to \pi^-\pi^-\pi^+\pi^+pp$ reactions.

A huge background contribution can be suppressed by tagging the ^{2}He nucleus. Fig. 24 shows the efficiency of $\pi^-\pi^-\pi^+\pi^+pp$ detection for the ^{2}He-formed events. The acceptance curve as a function of M_X is distorted by requiring ^{2}He formation but the oder of the

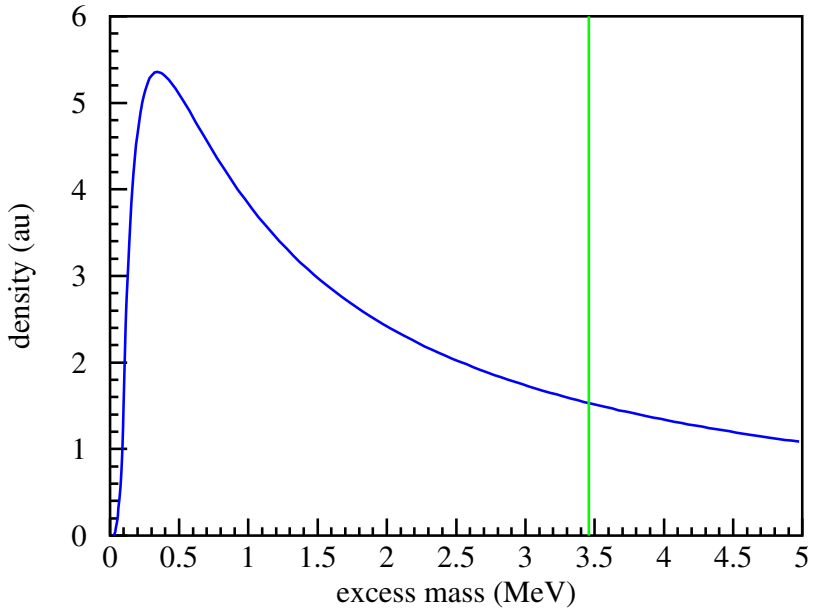

FIG. 22. Mass excess distribution of the ^{2}He nucleus (the diproton state). The excess is given by subtracting the sum of two proton masses from the ^{2}He mass. The mass distribution is calculated using the scattering length of $a_{pp} = -17.3$ fm and effective range of $r_{pp} = 2.85$ fm [64]. The vertical line (green) corresponds to the ^{2}He mass of 1.88 GeV.

acceptances are the same at a mass of 2.38 GeV for the $\pi^-\pi^-\pi^+\pi^+pp$ phase-space and ^{2}He-formed events. By using the acceptance for the ^{2}He-formed events, we estimated the missing mass M_X distributions for the $pp \to \pi^-\pi^-\mathcal{D}_{30}^{++++}$ and background $pp \to \pi^-\pi^-\pi^+\pi^+pp$ reactions. Fig. 25 shows the missing mass M_X distributions for the $pp \to \pi^-\pi^-\pi^+\pi^+pp$ reactions at 2.85, 3.35, 3.60, 3.80, and 4.00 GeV/c where the ^{2}He nucleus is required to be detected. When the branching ratio of $\mathcal{D}_{30}$ is assumed to be 1/3, the ^{2}He tagging reduce the signal yield by 1/7.3, giving a higher S/N ratio only at two lowest incident momenta, and a slightly higher ratio at the other momenta. The S/N ratios are 0.38, 0.42, 0.40, 0.47, and 0.37 for the 2.25–2.45-GeV events at 2.85, 3.35, 3.60, 3.80, and 4.00 GeV/c, respectively. The estimated statistical uncertainties are 0.004, 0.003, 0.002, and 0.002 GeV for the mass determination using the ^{2}He-tagged mass distributions at incident momenta of 3.35, 3.60, 3.80, and 4.00 GeV/c, respectively. While the those for the width are 0.021, 0.015, 0.011, and 0.011 GeV/c. Combining all the data acquired, the estimated statistical uncertainties become 0.001 and 0.004 GeV for the mass and width, respectively. Since the statistics become by a factor of approximately 1/10, the statistical uncertainties of mass and width

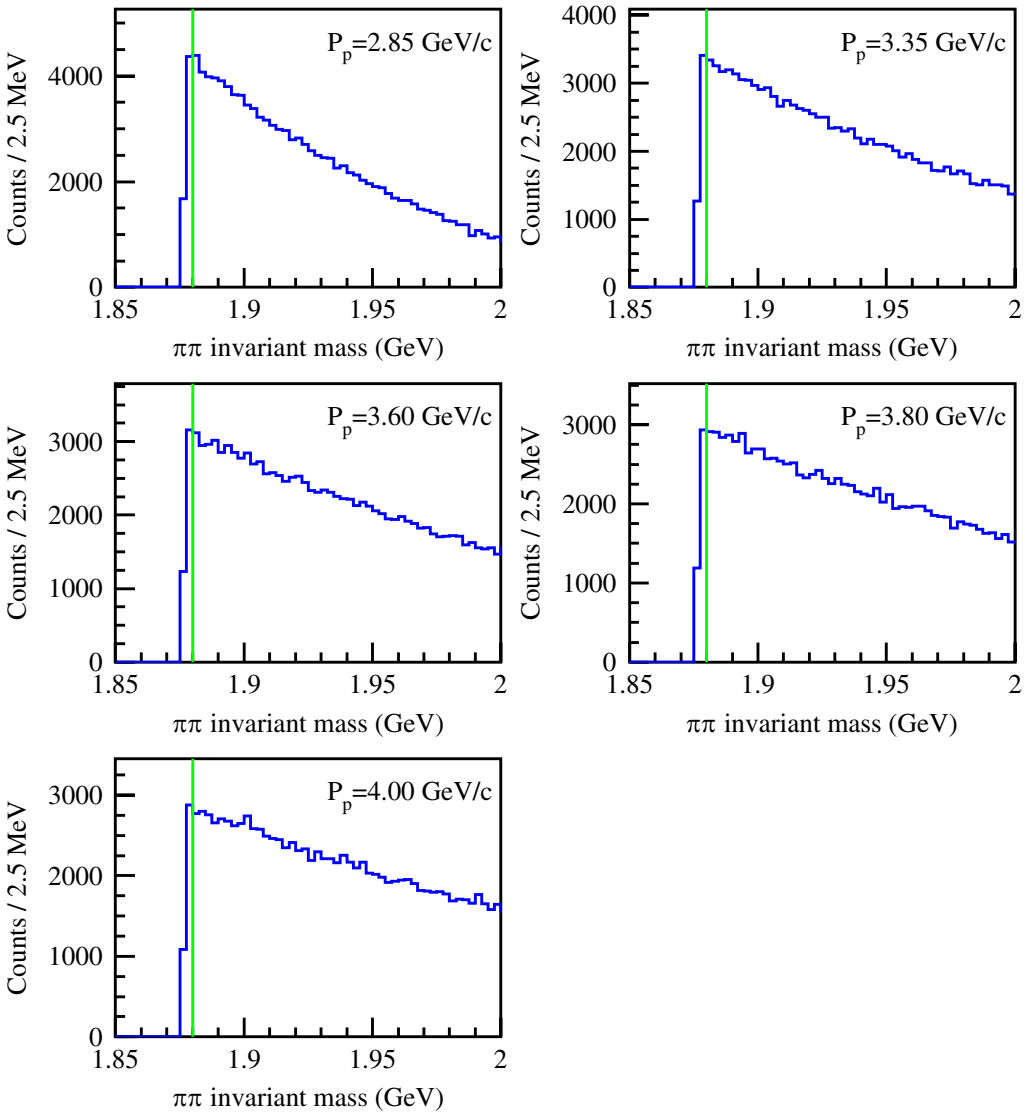

FIG. 23. pp invariant-mass distributions for the pure six-body phase-space $\pi^-\pi^-\pi^+\pi^+pp$ events at 2.85, 3.35, 3.60, 3.80, and 4.00 GeV/c. When the pp invariant mass is required to be less than 1.88 GeV as indicated by the vertical lines (green), the background contributions are reduced at $p(p,\pi^-\pi^-)$ missing mass of $\sim$ 2.38 GeV by a factor of 1/30.0, 1/32.3, 1/33.6, 1/40.2, and 1/33.9 at incident momenta of 2.85, 3.35, 3.60, 3.80, and 4.00 GeV/c, respectively.

determination are slightly larger than those without ^{2}He tagging. However, this ^{2}He-tagging method can be useful to find a possible $\mathcal{D}_{30}^{++++}$ contribution.

We request the three-day measurement of cross sections for the $pp \to \pi^-\pi^-\pi^+\pi^+pp$ reaction at each incident momenta of 3.35, 3.60, 3.80, and 4.00 GeV/c to find a possible $\mathcal{D}_{30}$ dibaryon and investigate its decay. Table VII summarizes the number of $\mathcal{D}_{30}^{++++}$-produced

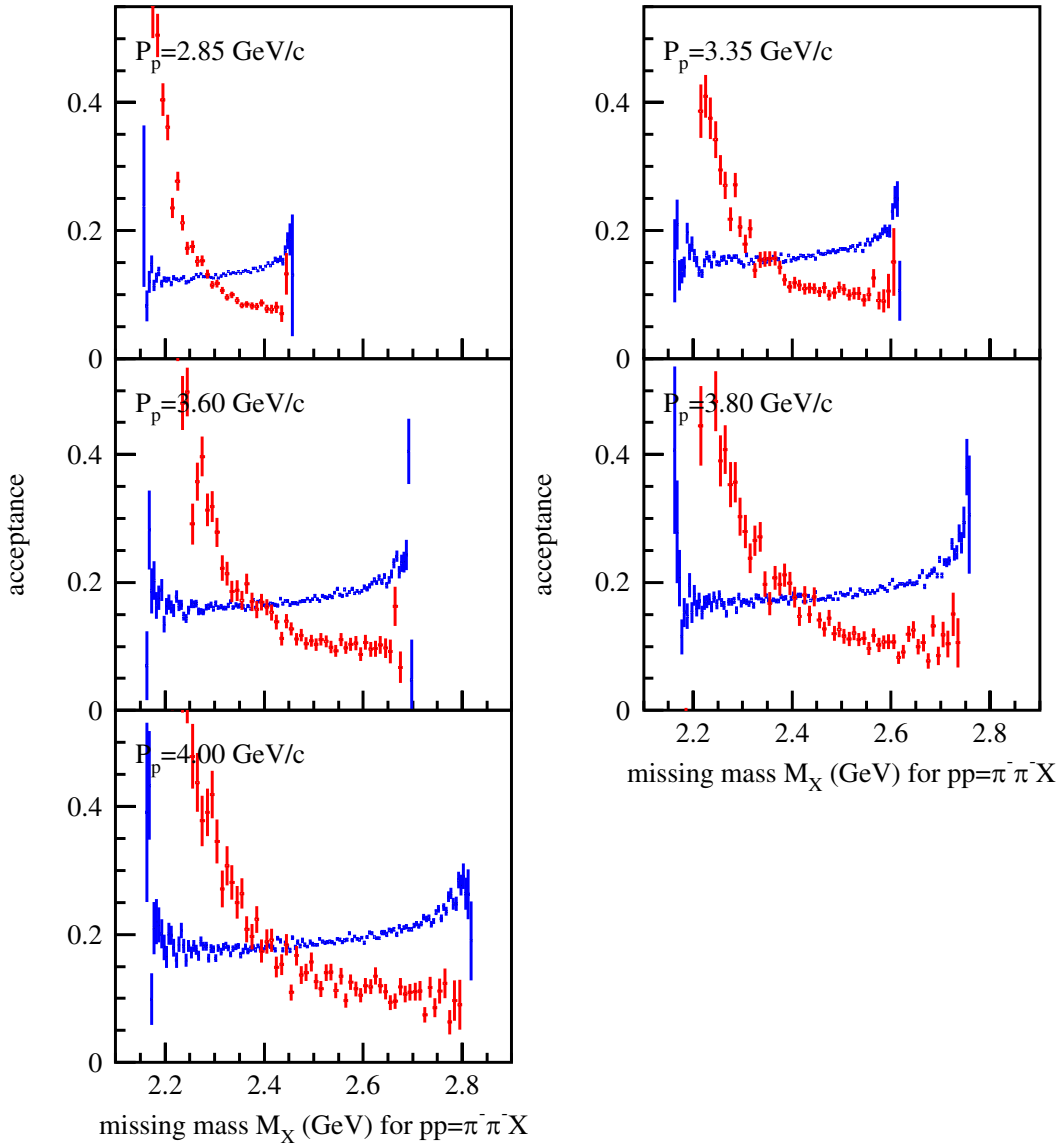

FIG. 24. Geometrical acceptances of $\pi^-\pi^-\pi^+\pi^+pp$ detections as a function of M_X for the $pp \to \pi^-\pi^-X$ reaction. The efficiencies are plotted for the pure six-body phase-space $\pi^-\pi^-\pi^+\pi^+pp$ events (blue), and ^{2}He-formed events (red).

events obtained in three days for all the $\pi^-\pi^-\pi^+\pi^+pp$-detected events and ^{2}He-tagging events.

We consider the thickness of the liquid hydrogen target is 570 mm. If it is shorter than we plan, an additional beam time is required. The high-intensity high-momentum secondary beamline is expected to be constructed step by step. Since the required beam intensity of protons is only 1 MHz, corresponding to the 0.5-kW loss (1/30 of the final goal) of the

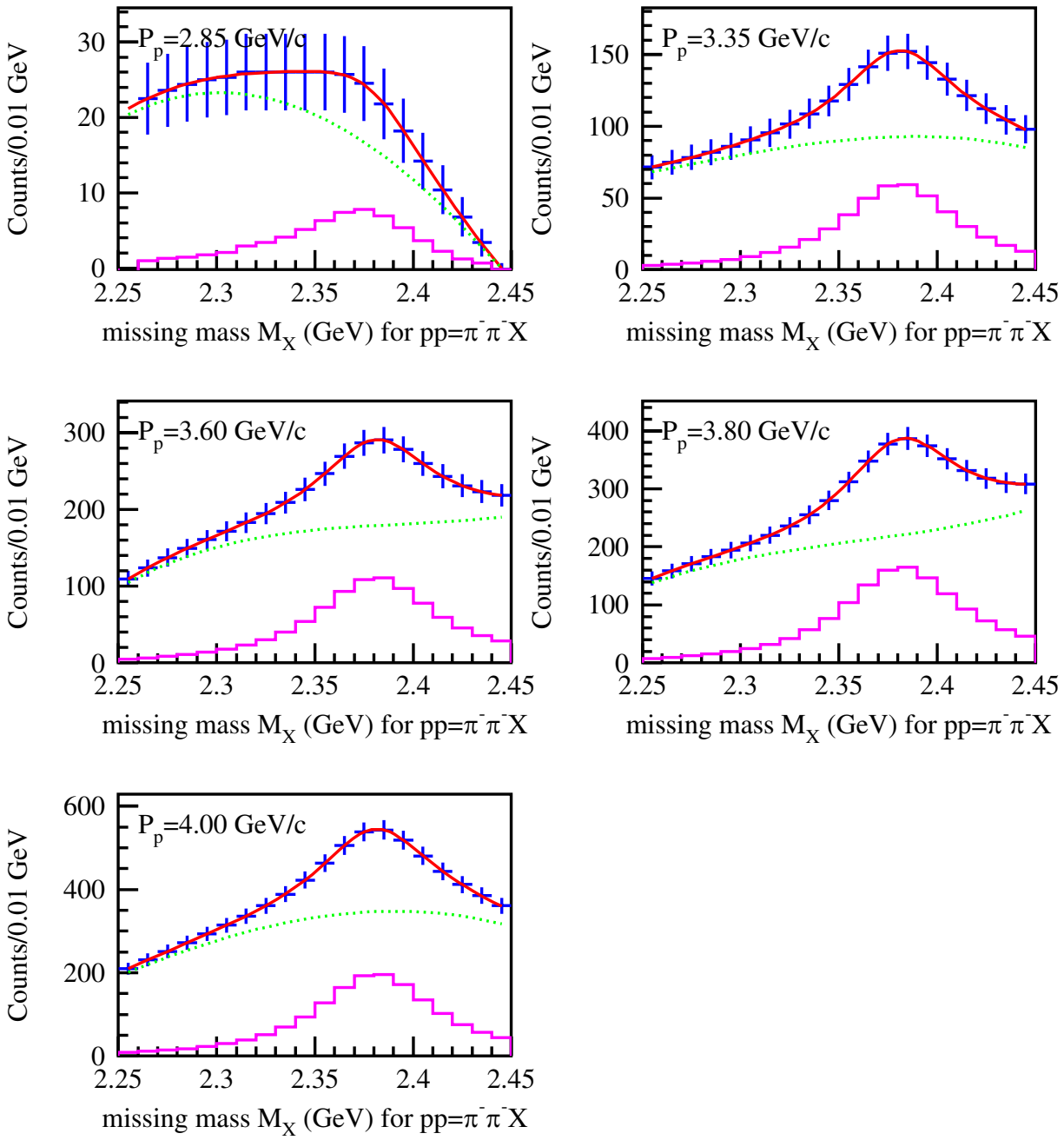

FIG. 25. Missing mass M_X distributions for the $pp \to \pi^-\pi^-\pi^+\pi^+pp$ reactions at 2.85, 3.35, 3.60, 3.80, and 4.00 GeV/c where the ^{2}He nucleus is required to be detected. The markers correspond to the expected experimental data obtained in a three-day measurement for all the incident momenta. In each panel, the solid curve (red) shows the fitted function expressed by a sum of the $\mathcal{D}_{30}$ production and background phase-space contributions. The histogram (magenta) represents the extracted $\mathcal{D}_{30}$ contribution, and the dotted curve (green) shows the background contribution.

TABLE VII. Estimated numbers of $\mathcal{D}_{30}^{++++}$-produced events obtained in three days for all the $\pi^-\pi^-\pi^+\pi^+pp$-detected events and ^{2}He-tagging events. Not only the geometrical acceptances but also DAQ, tracking, and particle-identification efficiencies are taken into account.

incident momentum (GeV/c)	2.85	3.35	3.60	3.80	4.00
all	320	2,900	5,200	8,300	10,000
^{2}He tagging	41	380	730	1,100	1,300

primary beam at the production target, the proposed experiment can be performed before the E50 experiment becomes ready.

Even if we do not observe $\mathcal{D}_{30}$, we can investigate the $\Delta^{++}\Delta^{++}$ interaction alternatively as described in §A, the $d^*(2380)$ production mechanism in the pp collision ($pp \to \pi^+ d^*(2380)$) as shown in §B, and the detailed studies of the produced $\mathcal{D}_{21}$ dibaryon via the $pp \to \pi^- (\pi^+\pi^+ p)$ reaction as briefly discussed in §C. It is important to measure cross sections at several incident momenta for studying the background, and confirming a possible $\mathcal{D}_{30}^{++++}$ contribution when we observe some resonance-like behavior in $\pi^+\pi^+pp$ invariant-mass distributions.

V. SUMMARY

We express our interest to search for the $I = 3$ dibaryon state ($\mathcal{D}_{30}$) at the high-intensity high-momentum secondary beamline at J-PARC. The $\mathcal{D}_{30}^{++++}$ can be observed in the missing-mass spectrum of the $p(p, \pi^-\pi^-)X$ reaction, and the mass and width can be obtained when we use the incident momentum around 3.0–4.0 GeV/c. The isospin of $\mathcal{D}_{30}$ is also uniquely determined because the reaction only provides $I = 3$ state for the missing particle X. We acquire the data at incident momenta of 2,85, 3.35 3.60, 3.80, and 4.00 GeV/c for three days for each incident momentum using the general-purpose magnetic dipole-spectrometer prepared for the J-PARC E50 experiment. The expected numbers of the $\mathcal{D}_{30}^{++++}$ produced events are 2,900 and 310 within the mass region of 2.25–2.45 GeV at 3.35 GeV/c for all the $\pi^-\pi^-\pi^+\pi^+pp$-detected events and ^{2}He-tagging events, respectively. The estimated statistical uncertainties of the mass and width determination are expected to be 0.001 and 0.004 GeV assuming the mass of 2.38 GeV and width of 0.07 GeV, respectively. Since the background contribution is sensitive to the results and we don't know its details, it is crucial to acquire

data with different incident proton momenta. The first two incident momenta correspond to those the WASA-at-COSY collaboration used to search for $\mathcal{D}_{30}^{++++}$. Although the WASA-at-COSY collaboration did not get a clear evidence of $\mathcal{D}_{30}^{++++}$ owing to a lack of statistics coming from the very small acceptance for $\pi^-\pi^-\pi^+\pi^+pp$ detection owing to the low particle-identification power, but they observed an enhancement corresponding to $\mathcal{D}_{30}$. Therefore, the first two incident momenta are important to check this hint. When the existence of the $\mathcal{D}_{30}$ is confirmed, all the sextet (ground state) dibaryons are established. The measured mass and width also provide information on the $\Delta\Delta$ interaction.

Appendix A: $\Delta^{++}\Delta^{++}$ interaction

When we observe $\mathcal{D}_{30}^{++++}$, its mass and width provide information on $\Delta^{++}\Delta^{++}$ interaction. Even if we do not observe $\mathcal{D}_{30}^{++++}$, we can extract information on $\Delta^{++}\Delta^{++}$ interaction from the $\Delta^{++}\Delta^{++}$ invariant-mass distribution. We calculate the $\Delta^{++}\Delta^{++}$ invariant-mass distributions distorted by the final-state interaction between two Δ^{++} baryons using a Migdal-Watson formula [61, 62] with different scattering parameters. Fig. 26 shows the

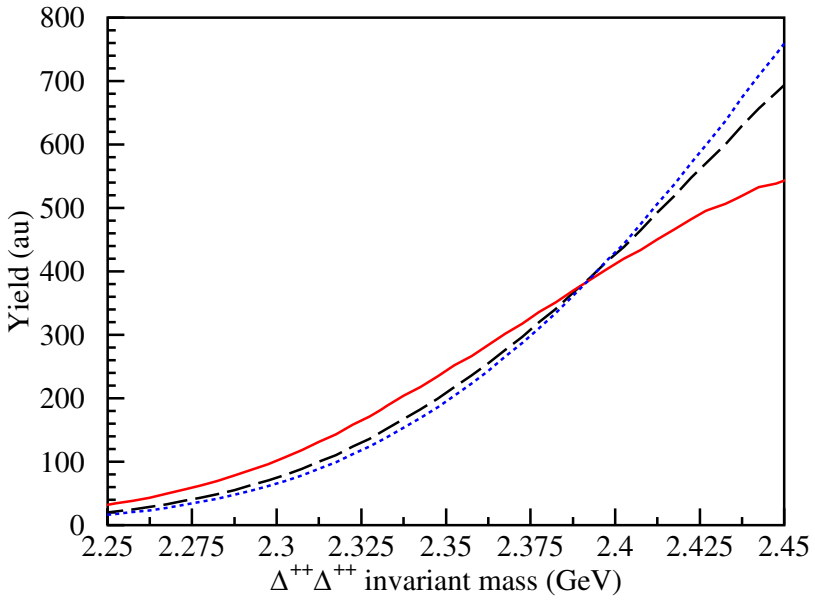

FIG. 26. $\Delta^{++}\Delta^{++}$ invariant-mass distributions for different phase shifts. The dashed curve (black) shows the non-interaction case, and the solid (red) and dotted (blue) represent the $\Delta\Delta$ interaction cases for $(I, J) = (0, 3)$ and $(3, 0)$ given by Oka and Yazaki [36].

$\Delta^{++}\Delta^{++}$ invariant mass distributions at incident proton momentum of 4.0 GeV/c. We employ the phase shifts for the $\Delta\Delta$ interaction with $(I, J) = (0, 3)$ and $(3, 0)$ given by Oka and Yazaki [36]. The corresponding scattering length a and effective range r are 1.88 and 0.93 fm, giving bound state, for $(I, J) = (0, 3)$, and 0.19 and 0.89 fm, giving no state, for $(I, J) = (3, 0)$. Different shapes are obtained between 2.25–2.45 GeV/c for the $\Delta^{++}\Delta^{++}$ invariant-mass distributions. The attractive $(I, J) = (0, 3)$ interaction gives convex upward, and repulsive $(3, 0)$ case gives concave. The detailed shape of the experimental obtained $\Delta^{++}\Delta^{++}$ distribution gives information on $\Delta^{++}\Delta^{++}$ interaction.

Appendix B: $d^*(2380)$ production via the $pp \to \pi^+(\pi^-\pi^+d)$ reaction

We can measure the cross sections for $d^*(2380)$ production via the $pp \to \pi^+(\pi^-\pi^+d)$ reaction if we loose the trigger condition so that we can obtain the events containing four charged particles. The angular distribution of $d^*(2380)$ production provides a hint on the internal structure of $d^*(2380)$. We can easily identify the $d^*(2380)$-produced events if the total cross section is large enough since the deuteron tagging makes the background very small as shown in Figs. 3 and 4.

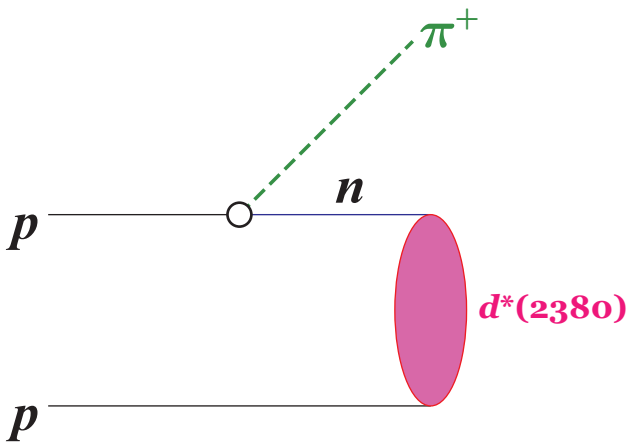

FIG. 27. Possible diagram for $d^*(2380)$ ($\mathcal{D}_{03}$) production from the pp collision: $pp \to \pi^+ d^*(2380)$. Once a proton is converted into neutron by emitting a positive pion, the np collision which is likely to produce $d^*(2380)$ can take place.

Here, the order estimation of the total cross sections are made using a simple model with an assumption of the sequential $pp \to \pi^+ (np) \to \pi^+ d^*(2380)$ process as shown in Fig. 27.

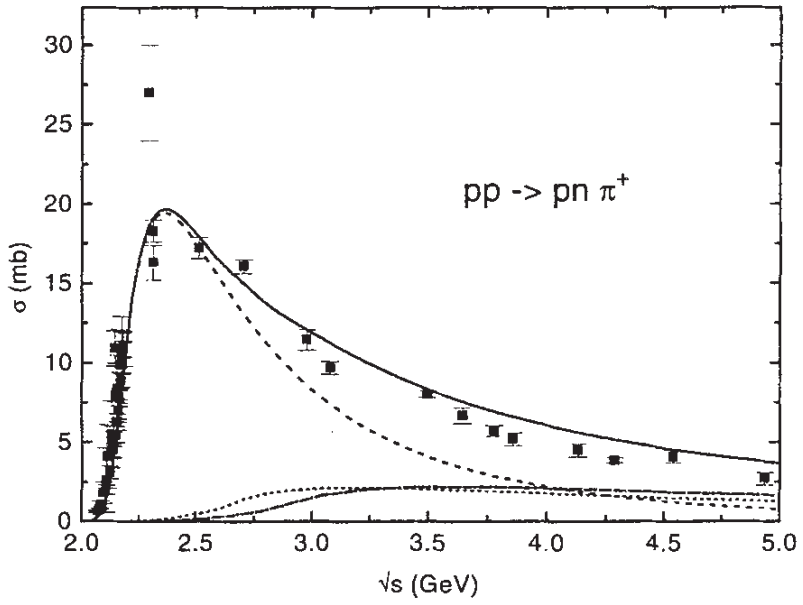

FIG. 28. Total cross section as a function of the CM energy for the $pp \to \pi^+ np$ reaction. The dotted curve shows the theoretical calculation only taking into account the baryon resonance in the intermediate state. The solid curve shows that adding the direct pion production in the proton-proton collision.

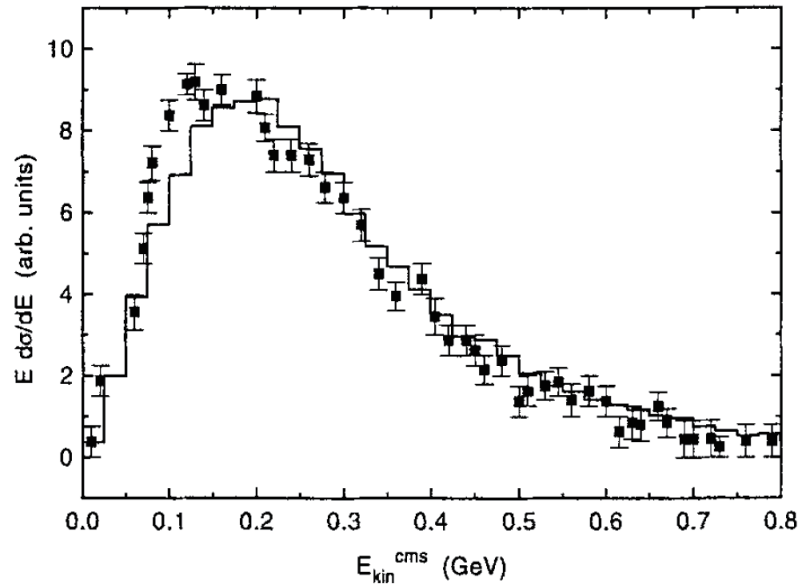

FIG. 29. Differential cross section $Kd\sigma/dK$ as a function of the pion kinetic energy K. The central events are selected that the impact parameter b is less than 2.1 fm. The solid curve shows the theoretical calculation. We obtain a simple approximate function: $Kd\sigma/dK \propto 0.18570\{(K/\mathrm{GeV}) + 24.579(K/\mathrm{GeV})^2\} \exp\{6.0819 - 12.872(K/\mathrm{GeV}) + 3.2270(K/\mathrm{GeV})^2\}$.

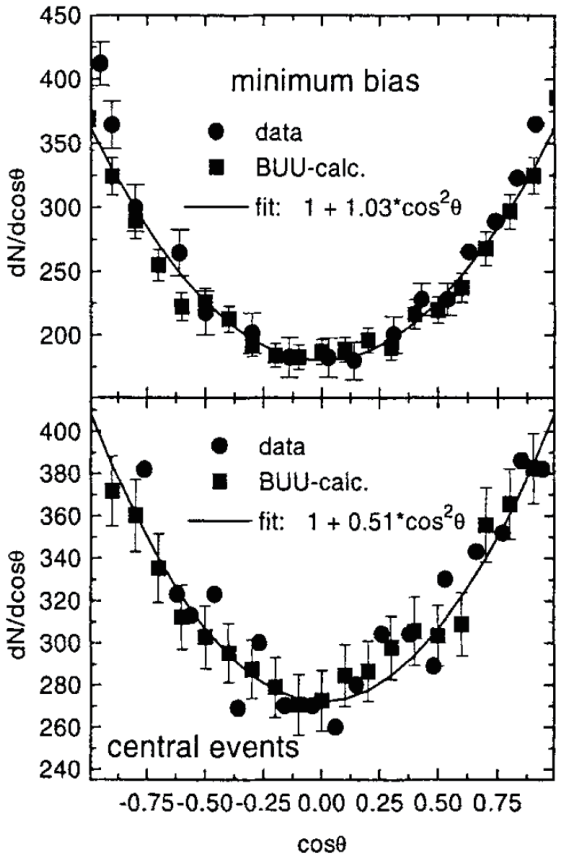

FIG. 30. Angular distributions of pion emission as a function of $\cos\theta$ in the CM frame for all the events (upper) and for the central events (lower). The filled circles show the experimental data, and squares show the theoretical calculations. The solid curve represents the fitted function in a form $1 + \alpha \cos^2\theta$ described in each panel.

As for the first-step $pp \to \pi^+ np$ process, we take the total cross section as a function of the CM energy, the differential cross section as a function of the pion kinetic energy, and the angular distribution of pion emission from Ref. [65]. Fig. 28 shows the total cross section as a function of the CM energy for the $pp \to \pi^+ np$ reaction. The total cross section of the first step is given from Fig. 28. Fig. 29 shows the differential cross section $K d\sigma/dK$ as a function of the pion kinetic energy K in the CM frame. It should be noted that the absolute values are not provided in Fig. 29. We obtain a simple approximate form:

$$K\frac{d\sigma}{dK} \propto 0.18570 \left\{ \left(\frac{K}{\mathrm{GeV}}\right) + 24.579 \left(\frac{K}{\mathrm{GeV}}\right)^2 \right\} \times \exp\left\{ 6.0819 - 12.872 \left(\frac{K}{\mathrm{GeV}}\right) + 3.2270 \left(\frac{K}{\mathrm{GeV}}\right)^2 \right\}, \tag{B1}$$

and use this for all the incident momenta with a normalization factor of $1/\int_0^\infty (d\sigma/dK)\,dK = 17.17$. Fig. 30 shows the angular distribution of pion emission in the CM frame. We use a form $1 + 0.51\cos^2\theta$ for all the incident momenta. The first-step process leaves the np system in the final state. According to the formation cross section of $d^*(2380)$ from the pn collision, we can give the probability of $d^*(2380)$ formation in $pp \to \pi^+ pn$. The formation cross section is simply given by the Breit-Wigner formula with a mass of 2.37 GeV and width of 0.07 GeV, and is 0.44 mb at the centroid mass. Here, the cross section includes the branching ratio of $\sim 23\%$ for $\mathcal{D}_{03} \to \pi^+\pi^- d$, namely the actual formation cross section of $\mathcal{D}_{03}$ is 4.3 times larger than described. The formation probability is calculated in the following way: a point-like neutron is produced according to the proton charge density in the first step process; the neutron travels in a proton with an exponential density, corresponding to the dipole form factor, with a radius of 0.85 fm; and the formation probability in a unit travel length is given by a multiplication of the formation cross section and proton number density. The penetration lengths are different for different initial positions of produced neutrons. We obtain the total cross section from the multiplication between that for the first step and average formation probability.

The obtained total cross sections are 2.4, 1.7, 1.1, 0.70, and 0.48 μb for $d^*(2380)$ at incident momenta of 2.85, 3.35, 3.6, 3.8, and 4.0 GeV/c, respectively. The total cross section is larger for the lower incident momentum. Those are 0.037, 0.27, 0.50, 0.73, and 0.97 μb for $\mathcal{D}_{30}^{++++}$, and the order of cross sections are similar between $d^*(2380)$ and $\mathcal{D}_{30}^{++++}$ production at high incident momenta. At the lower incident momentum, the total cross section is much higher for $\mathcal{D}_{03}$ production. Since the $d^*(2380)$-produced events contain only four charged tracks in the final state, the tracking efficiency, particle-identification efficiency, and geometrical acceptance are much higher than those for $\mathcal{D}_{30}^{++++}$ production. Furthermore, the background contributions are reduced significantly by the deuteron tagging. The byproduct measurement of cross sections for $d^*(2380)$ production is considered to be much easier.

Appendix C: $\mathcal{D}_{21}$ production via the $pp \to \pi^- (\pi^+ pp)$ reaction

The isotensor dibaryon $\mathcal{D}_{21}$ was observed by the WASA-at-COSY collaboration by using the $pd \to \pi^- (\pi^+ pp)\, n_{\rm spectator}$ reaction. The incident energy of the proton beam was $T_p = 1.2$ GeV, corresponding to the incident momentum of 1.92 GeV/c, and effectively covered from

1.08 to 1.36 GeV (from 1.79 to 2.10 GeV/c) for the $pp \to \pi^-\pi^+pp$ reaction. Since charge identification and momentum determination with a magnetic field were available only for the central detector in WASA, they required that the two protons were detected with the forward detector, and that the other two charged pions were detected with the central detector. Using the E50 spectrometer together with the higher incident momentum, the acceptance for $\pi^-\pi^+pp$ detection including particle detection becomes much higher, and we can study the π^+pp invariant-mass distribution with less acceptance bias. The total cross section for $\mathcal{D}_{21}^{+++}$ production is much higher [33] by a factor of 100–1,000 than that for $\mathcal{D}_{30}^{++++}$ production. Thus, the byproduct measurement of cross sections for $\mathcal{D}_{21}^{+++}$ production is considered to be much easier.

---

[1] H. Clement, Prog. Part. Nucl. Phys. **93**, 195 (2017).

[2] H. Shen, H. Toki, K. Oyamatsu, and K. Sumiyoshi, Nucl. Phys. A **637**, 435 (1998).

[3] F.J. Dyson and N.-H. Xuong, Phys. Rev. Lett. **13**, 815 (1964).

[4] B.S. Neganov, and L.B. Parfenov, J. Exp. Theor. Phys. **7**, 528 (1958).

[5] R.A. Arndt, I.I. Strakovsky, and R.L. Workman, Phys. Rev. C **50**, 1796 (1994).

[6] R.A. Arndt, I.I. Strakovsky, R.L. Workman, and D.V. Bugg, Phys. Rev. C **48**, 1926 (1993).

[7] C.H. Oh, R.A. Arndt, I.I. Strakovsky, and R.L. Workman, Phys. Rev. C **56**, 635 (1997).

[8] T. Ishikawa *et al.*, Phys. Lett. B **789**, 413 (2019).

[9] T. Kamae *et al.*, Phys. Rev. Lett. **38**, 468 (1977).

[10] T. Kamae and T. Fujita, Phys. Rev. Lett. **38**, 471 (1977).

[11] M. Bashkanov *et al.*, Phys. Lett. B **789**, 7 (2019).

[12] M. Bashkanov *et al.* (CELSIUS/WASA collaboration), Phys. Rev. Lett. **102**, 052301 (2009).

[13] P. Adlarson *et al.* (WASA-at-COSY collaboration), Phys. Rev. Lett. **106**, 242302 (2011).

[14] A. Abashian, N.E. Booth, and K.M. Crowe, Phys. Rev. Lett. **5**, 258 (1960).

[15] N.E. Booth, A. Abashian, and K.M. Crowe, Phys. Rev. Lett. **7**, 35 (1961).

[16] M. Bashkanov, and H. Clement, Eur. Phys. J. A **50**, 107 (2014).

[17] G. Agakichiev *et al.* (CERES collaboration), Phys. Lett. B **422**, 405 (1998).

[18] P. Adlarson *et al.* (WASA-at-COSY collaboration), Phys. Lett. B **721**, 229 (2013).

[19] P. Adlarson *et al.* (WASA-at-COSY collaboration), Phys. Rev. C **88**, 055208 (2013).

[20] P. Adlarson, et al. (WASA-at-COSY collaboration), Phys. Lett. B **743**, 325 (2015).

[21] H. Clement, M. Bashkanov, and T. Skorodko, Phys. Scr. **T166**, 014016 (2015).

[22] P. Adlarson *et al.* (WASA-at-COSY collaboration, SAID Data Analysis Center), Phys. Rev. Lett. **112**, 202301 (2014).

[23] P. Adlarson *et al.* (WASA-at-COSY Collaboration, SAID Data Analysis Center), Phys. Rev. C **90**, 035204 (2014).

[24] A. Gal, and H. Garcilazo, Phys. Rev. Lett. bf 111, 172301 (2013).

[25] Y. Dong, P. Shen, F. Huang, Z. Zhang, Phys. Rev. C **91** (2015) 064002.

[26] F. Huang, Z.Y. Zhang, P.N. Shen, and W.L. Wang, arXiv: 1408.0458 (2014).

[27] F. Huang, P.N. Shen, Y.B. Dong, and Z.Y. Zhang, arXiv: 1505.05395 (2015).

[28] M.N. Platonova, and V.I. Kukulin, Nucl. Phys. A **946**, 11 (2016).

[29] R.A. Schumacher, talk at Meson in Nucleus 2016 (MIN16) (2016);
MIN16 website: ⟨http://www2.yukawa.kyoto-u.ac.jp/˜min2016/⟩.

[30] T. Ishikawa *et al.*, Phys. Lett. B **772**, 398 (2017).

[31] A. Fix, and H. Arenhövel, Euro. Phys. J. A **25**, 115 (2005).

[32] M. Egorov, and A. Fix, Nucl. Phys. A **933**, 104 (2015).

[33] P. Adlarson *et al.* (WASA-at-COSY collaboration), Phys. Rev. Lett. **121**, 052001 (2018).

[34] P. Adlarson *et al.* (WASA-at-COSY collaboration), Phys. Lett. B **762**, 455 (2016).

[35] P.J.G. Mulders, A.Th.M. Aerts, J.J. de Swart, Phys. Rev. D **21**, 2653 (1980).

[36] M. Oka and K. Yazaki, Phys. Lett. B **90**, 41 (1980).

[37] P.J. Mulders, A.W. Thomas, J. Phys. G **9**, 1159 (1983).

[38] A. Gal and H. Garcilazo, Nucl. Phys. A **928**, 73 (2014).

[39] S. Gongyo *et al.* (HAL QCD collaboration), Phys. Rev. Lett. **120**, 212001(2018).

[40] N. Ishii, S. Aoki, and T. Hatsuda, Phys. Rev. Lett. **99**, 022001 (2007).

[41] H. Noumi *et al.*, "*Charmed Baryon Spectroscopy via the* (π, D^{*-}) *reaction*, " Proposals for the J-PARC experiment, J-PARC P50 (2013): ⟨`http://j-parc.jp/researcher/Hadron/en/pac_1301/pdf/P50_2012-19.pdf`⟩.

[42] H. Noumi, Few-Body Syst. **54**, 813 (2013).

[43] K. Shirotori *et al.*, PoS(Hadron 2013)130 (2014).

[44] H. Noumi, PoS(Hadron 2013)031 (2014).

[45] K. Shirotori *et al.*, JPS Conf. Proc. **8**, 022012 (2015).

[46] T.N. Takahashi for the J-PARC E50 collaboration, JPS Conf. Proc. **13**, 020042 (2017).

[47] H. Noumi, JPS Conf. Proc. **13**, 010017 (2017).

[48] H. Noumi, JPS Conf. Proc. **17**, 111003 (2017).

[49] Y. Komatsu *et al.*, JPS Conf. Proc. **26**, 022029 (2019).

[50] H. Takahashi, private communication.

[51] J.R. Sanford, and C.L. Wang, BNL 11279 and BNL 11479 (1967).

[52] C.L. Wang, Phys. Rev. Lett. **25**, 1068 (1970).

[53] K.H. Tanaka *et al.*, Nucl. Intrum. Meth. A **363**, 114 (1995).

[54] Y. Ma *et al.*, "*Performance evaluation of the next generation DAQ system with high-rate detectors for the J-PARC E50 experiment*," Proposals for the ELPH experiment, ELPH-2900 (2018).

[55] Chr. Bargholtz *et al.* (CELSIUS/WASA collaboration), Nucl. Intrum. Meth. A **594**, 339 (2008).

[56] S. Agostineli *et al.*, Nucl. Instrum. Meth. A **506**, 250 (2003).

[57] J. Allison *et al.*, IEEE Trans. Nucl. Sci. **53**, 270 (2006).

[58] Geant4 website: ⟨`http://geant4.cern.ch/`⟩.

[59] M. Bashkanov, private communication.

[60] M. Bashkanov, H. Clement, and T. Skorodko, Eur. Phys. J. A **51**, 87 (2015).

[61] K.M. Watson, Phys. Rev. **88**, 1163 (1952).

[62] A.B. Migdal, Sov. Phys. JETP **1**, 2 (1955).

[63] S. Dymov *et al.*, Phys. Lett. **635**, 270 (2006).

[64] G.A. Miller, M.K. Nefkens, and I. Šlaus, Phys. Rep. **194**, 1 (1990).

[65] S. Teis *et al.*, Z. Phys. A **356**, 421 (1997).